© 2022. Published by The Company of Biologists Ltd | Journal of Cell Science (2022) 135, jcs259380. doi:10.1242/jcs.259380

RESEARCH ARTICLE

RNA-assisted sequestration of RNA-binding proteins by cytoplasmic inclusions of the C-terminal 35-kDa fragment of TDP-43

Lei-Lei Jiang[1,*], Wen-Liang Guan[1,2,*], Jian-Yang Wang[1,2], Shu-Xian Zhang[1,2] and Hong-Yu Hu[1,‡]

ABSTRACT

TDP-43 (also known as TARDBP) is a nuclear splicing factor functioning in pre-mRNA processing. Its C-terminal 35-kDa fragment (TDP-35) forms inclusions or aggregates in cytoplasm, and sequesters full-length TDP-43 into the inclusions through binding with RNA. We extended the research to investigate whether TDP-35 inclusions sequester other RNA-binding proteins (RBPs) and how RNA-binding specificity has a role in this sequestration process. We have characterized T-cell restricted intracellular antigen-1 (TIA1) and other RBPs that can be sequestered into the TDP-35 inclusions through specific RNA binding, and found that this sequestration leads to the dysfunction of TIA1 in maturation of target pre-mRNA. Moreover, we directly visualized the dynamic sequestration of TDP-43 by the cytoplasmic TDP-35 inclusions by live-cell imaging. Our results demonstrate that TDP-35 sequesters some specific RBPs and this sequestration is assisted by binding with RNA in a sequence-specific manner. This study provides further evidence in supporting the hijacking hypothesis for RNA-assisted sequestration and will be beneficial to further understanding of the TDP-43 proteinopathies.

KEY WORDS: TDP-43, RNA-assisted sequestration, RNA-binding protein, TIA1, Cytoplasmic inclusion, Live-cell imaging

INTRODUCTION

Protein misfolding, aggregation or inclusion formation is a pathological hallmark of neurodegenerative diseases (NDs) (Chiti and Dobson, 2017; Dugger and Dickson, 2017; Hartl, 2017). RNA-binding proteins (RBPs) are widely implicated in the pathogenesis of the NDs (Hofmann et al., 2019; Kim et al., 2021; Mackenzie et al., 2017; Nussbacher et al., 2019; Xue et al., 2020b). These RBPs commonly have one or multiple RNA-binding domains (Clery et al., 2008; Helder et al., 2016) and intrinsically disordered regions (IDRs) (Calabretta and Richard, 2015; Franzmann and Alberti, 2019) in their sequences, and some RBPs contain prion-like domains responsible for amyloid aggregation and inclusion formation (Harrison and Shorter, 2017; Picchiarelli and Dupuis, 2020). Among them, TAR DNA binding protein of 43 kDa (TDP-43; also known as TARDBP), a nuclear splicing factor (Buratti and Baralle, 2010), has been revealed to be the major component of the inclusions associated with amyotrophic lateral sclerosis (ALS) and frontotemporal lobar dementia (FTLD) (Arai et al., 2006; Chen and Mitchell, 2021; Neumann et al., 2006). TDP-43 is composed of an N-terminal domain (NTD), two RNA recognition motifs (RRMs) and the C-terminal IDRs, wherein most genetic mutations occur (Lagier-Tourenne and Cleveland, 2009). The NTD domain mediates formation of a homodimer that plays a role in promoting pre-mRNA splicing and inhibits TDP-43 aggregation in cells (Jiang et al., 2017; Mompean et al., 2017; Vivoli-Vega et al., 2020). Truncation of the NTD (Nishimoto et al., 2010) or alternative translation (Xiao et al., 2015) can generate the C-terminal 35-kDa fragment of TDP-43 (TDP-35, residues 85–414 or 90–414), which leads to formation of the cytoplasmic inclusions (Che et al., 2011). The two RRM domains are responsible for binding to UG-rich RNA and TG-rich DNA targets (Passoni et al., 2012), with the RNA-binding ability being important for TDP-43 aggregation and inclusion formation (Ayala et al., 2005; Buratti and Baralle, 2001; Huang et al., 2013; Ihara et al., 2013). The C-terminal IDRs includes two glycine-rich regions (GRRs), an amyloidogenic core (AC) (Jiang et al., 2013) and a Q/N-rich region (Budini et al., 2012), which participate in protein interaction and/or protein aggregation (Buratti et al., 2005; Pesiridis et al., 2011; Smethurst et al., 2015). Normally, TDP-43 is predominantly localized in the nucleus and plays multiple functions in transcription, pre-mRNA splicing, regulation of RNA stability and translation (Bhardwaj et al., 2013; Buratti and Baralle, 2010; Freibaum et al., 2010; Tollervey et al., 2011). However, TDP-43 may undergo ubiquitylation, redistribution from nucleus to cytoplasm, fragmentation and aggregation or inclusion formation in the cytoplasm, and consequently lose its normal function, which results in pathological cases known as TDP-43 proteinopathies (Arai et al., 2006; Chen and Mitchell, 2021; Neumann et al., 2006; Suk and Rousseaux, 2020; Winton et al., 2008). In addition, TDP-43 is also involved in formation of the stress granules (SGs) in cultured cells and disease pathologies (Besnard-Guerin, 2020; Chen and Cohen, 2019).

So far, the pathological mechanism of TDP-43 proteinopathy has been investigated considerably (Cascella et al., 2016; Chen and Mitchell, 2021; Droppelmann et al., 2019; Picchiarelli and Dupuis, 2020; Wood et al., 2021). Mostly, the C-terminal fragments of TDP-43 have received more attention, which are implicated to be essential for TDP-43 aggregation and inclusion formation (Budini et al., 2012; Che et al., 2011; Chhangani et al., 2021; Gregory et al., 2012; Medina et al., 2014). As a pathologically derived C-terminal fragment of TDP-43, TDP-35 still retains its RNA-binding ability, but it may experience mis-localization to cytoplasm and formation of aggregates or inclusions, and consequently leads to alteration of RNA processing (Che et al., 2011; Nishimoto et al., 2010).

[1]State Key Laboratory of Molecular Biology, Shanghai Institute of Biochemistry and Cell Biology, Center for Excellence in Molecular Cell Science, Chinese Academy of Sciences, Shanghai 200031, P. R. China. [2]University of Chinese Academy of Sciences, Beijing 100049, P. R. China.
*These authors contributed equally to this work

‡Author for correspondence (hyhu@sibcb.ac.cn)

H.-Y.H., 0000-0001-9557-9841

Handling Editor: Maria Carmo-Fonseca
Received 15 September 2021; Accepted 31 January 2022

Journal of Cell Science (2022) 135, jcs259380. doi:10.1242/jcs.259380

Our previous research has demonstrated that TDP-35 triggers formation of cytoplasmic inclusions and sequesters full-length TDP-43 into inclusions through binding with RNA and ultimately alters the pre-mRNA splicing function of TDP-43 (Che et al., 2015, 2011). Considering the sequestration of TDP-43, we speculate that other RBPs may also be sequestered into the TDP-35 inclusions via binding with various RNA molecules. In consistent with the hijacking model we have proposed (Yang and Hu, 2016), RNA-assisted sequestration of the cellular interacting RBP partners by the cytoplasmic TDP-35 aggregates or inclusions may contribute to the pathogenesis of ALS/FTLD and other NDs.

Here, we further investigated whether the cytoplasmic TDP-35 inclusions sequester other RBPs and how RNA-binding specificity exerts an assisting action in this sequestration process. Several specific RBPs that can be sequestered into the cytoplasmic inclusions by TDP-35 in a process assisted by specific cellular RNA were identified. Moreover, the dynamic sequestration of TDP-43 by cytoplasmic TDP-35 inclusions was directly visualized in living cells. This study on the RNA-assisted sequestration of RBPs by the TDP-35 inclusions may open the avenue for deciphering TDP-43 proteinopathy in NDs.

RESULTS

Identification of the RNA-binding proteins sequestered by cytoplasmic TDP-35 inclusions

Our previous study demonstrated that TDP-35 can sequester full-length TDP-43 into cytoplasmic aggregates or inclusions and RNA plays a critical role in this sequestration process (Che et al., 2015). To identify other RBPs that might be sequestered by the TDP-35 inclusions, we performed immunofluorescence microscopic imaging to characterize their possible colocalization and sequestration in cultured cells. Normally, T-cell restricted intracellular antigen-1 (TIA1) is mainly localized in the nucleus (Kedersha et al., 1999) and cytoplasmic poly(A)-binding protein 1 (PABPC1) is in the cytoplasm (Afonina et al., 1998). Confocal microscopy imaging showed that some endogenous TIA1 molecules were colocalized with the cytoplasmic inclusions formed by TDP-35 in HEK 293T cells (Fig. 1A), which was accompanied with significant decrease of the TIA1 level in the nucleus, but this sequestration process was not observed with TDP-35-4FL, an RNA-binding deficient mutant (Buratti and Baralle, 2001; Che et al., 2015). Analogously, endogenous PABPC1 was also sequestered into the TDP-35 inclusions in the cytoplasm, and RNA-binding deficiency eliminated their colocalization (Fig. 1B). We also examined four other RBPs, and found that hnRNPA2/B1 (Liu and Shi, 2021), to some extent, colocalized with the TDP-35 inclusions in cytoplasm, but this was not observed with hnRNPA1 (Clarke et al., 2021), matrin-3 (Matr3) (Johnson et al., 2014) or PABPN1 (Banerjee et al., 2013) (Fig. S1). This observation that TDP-35 sequesters endogenous TIA1 and PABPC1 into cytoplasmic inclusions was also replicated in HeLa cells (Fig. S2A,B). Similar results were also obtained with exogenously overexpressed TIA1 and PABPC1 with these both being sequestered in the TDP-35 inclusions in HEK 293T cells (Fig. S2C,D). Thus, these data from immunofluorescence microscopy imaging demonstrate that the cytoplasmic TDP-35 inclusions can sequester some RBPs in an as-yet-unidentified manner.

TDP-35 sequesters TIA1 into cytoplasmic inclusions or aggregates

TIA1 is an RNA-binding protein mainly functioning as a regulator of pre-mRNA splicing and mRNA stability (Sanchez-Jimenez and Izquierdo, 2015). Our microscopy imaging revealed that TIA1 can be sequestered into the cytoplasmic inclusions formed by TDP-35. To further detail the molecular properties of sequestration, we performed a supernatant–pellet fractionation experiment on the lysates from HEK 293T cells overexpressing TDP-35. The results showed that TDP-35 formed insoluble aggregates that appeared in the pellet fraction and simultaneously sequestered more endogenous TIA1 into the aggregates (Fig. 1C,D). As a comparison, the TDP-35-4FL mutant formed fewer aggregates that appeared in the pellet, and the amount of sequestered TIA1 in the pellet was significantly reduced. To corroborate this finding, we performed a dose-dependent experiment in HeLa cells. We found that with an increased dose of TDP-35, the amount of insoluble TIA1 aggregates observed in the pellet fraction was gradually increased (Fig. S3), which was accompanied by an increase of the TDP-35 aggregates. However, this sequestration effect was abolished with the TDP-35-4FL mutation. Taken together, the cytoplasmic TDP-35 aggregates specifically sequester TIA1 and RNA binding is implicated in this sequestration process.

The TDP-35 aggregates sequester TIA1 through sequence-specific RNA interactions

It is known that TDP-35 sequesters TDP-43 into cytoplasmic inclusions through binding with poly(A)-containing RNA (i.e. mRNA) (Che et al., 2015), and RBPs and their bound RNAs are associated with the formation of SGs in cells (Rhine et al., 2020; Wolozin and Ivanov, 2019). In light of the importance of RNA binding, we presumed that specific RNA molecules might be essential for the sequestration of TDP-35 and other RBPs. To examine the role of specific RNA molecules in TDP-35 sequestration, we applied ribonuclease (RNase) and single-stranded DNA (ssDNA) treatments and performed supernatant–pellet fractionation experiment on the lysates from HEK 293T cells overexpressing TDP-35 (Fig. 2). The ssDNA fragments mimicking the corresponding RNA included TG repeats (TDP-43 and TDP-35 binding) (Lukavsky et al., 2013; Passoni et al., 2012), TC-rich sequences (TIA1 binding) (Waris et al., 2017) and their chimera TG+TC sequence (binding with TDP-35 and TIA1 simultaneously). Without RNase treatment, a large amount of TIA1 appeared in the pellet fraction with insoluble TDP-35. When the cell lysates were treated with RNase A for digesting RNA, the level of TDP-35 aggregates were reduced significantly, and as a result, the insoluble TIA1 in the pellet fraction disappeared substantially (Fig. 2A,C). Correspondingly, the soluble amount of TIA1, in the supernatant, was considerably increased (Fig. 2A,B). With addition of the TG repeat on the RNase-treated sample, the amounts of insoluble aggregates for both TDP-35 and TIA1 were increased slightly compared with the amount seen with RNase treatment only, but the TC-rich ssDNA had little effect on the level of these in the pellet. Interestingly, with addition of the chimera TG+TC ssDNA, the level of insoluble TIA1 in the pellet was remarkably recovered in contrast with what was seen with RNase treatment only (Fig. 2A,C), while the soluble amount in the supernatant was reduced slightly (Fig. 2A,B). This indicates that the chimeric ssDNA mediates the association of TDP-35 and TIA1, and assists sequestration of TIA1 by TDP-35. This finding implies that the RNAs of specific sequences are critically important to the sequestration of TIA1 by the TDP-35 aggregates. Note that the change of the insoluble TIA1 amount in the pellet is roughly parallel with that of TDP-35 upon various treatments, suggesting that sequestration of TIA1 by TDP-35 in turn enhances TDP-35 aggregation and that these two proteins may form aggregates cooperatively with the assistance of specific RNA.

Journal of Cell Science (2022) 135, jcs259380. doi:10.1242/jcs.259380

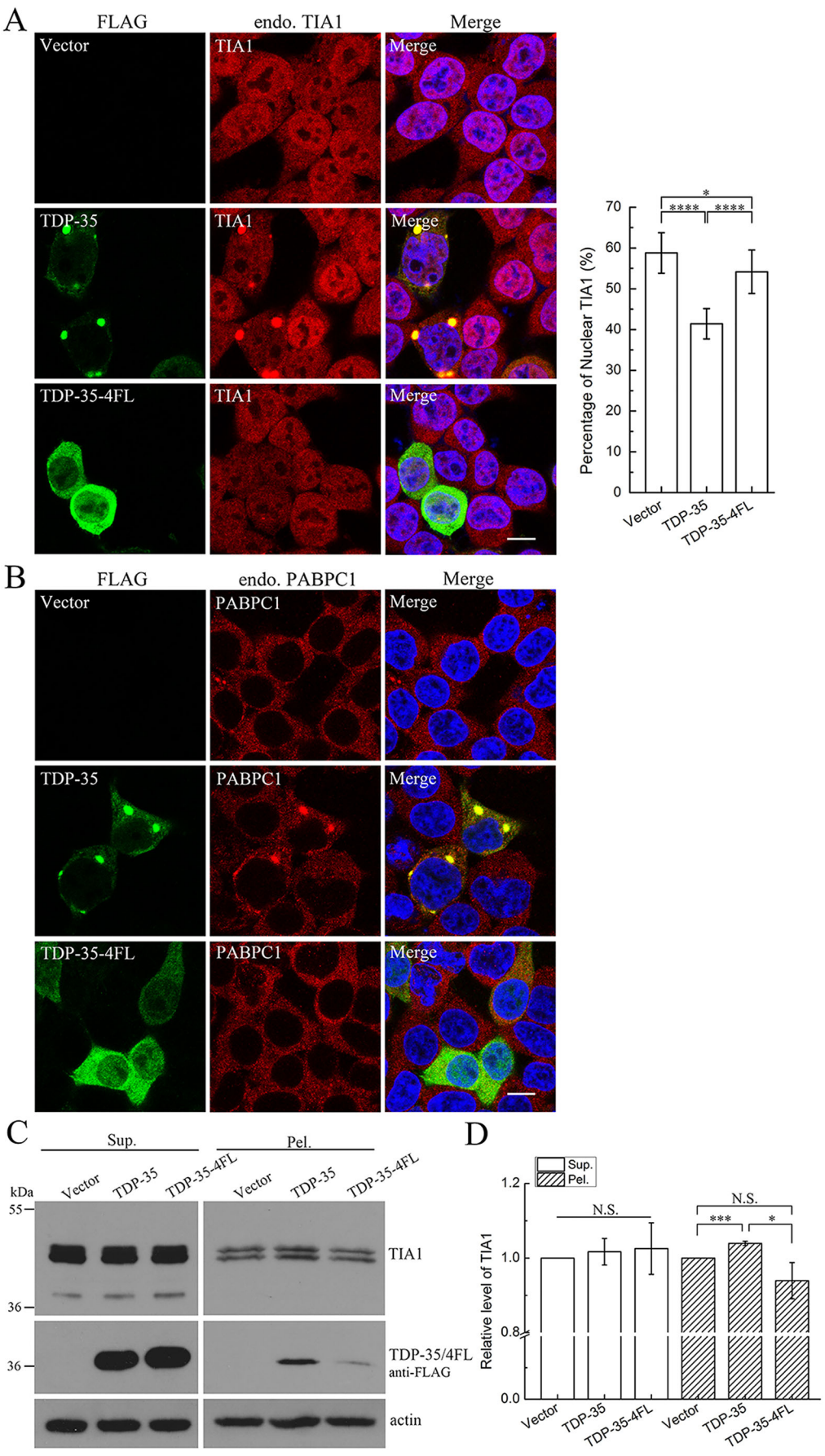

Fig. 1. Characterization of the RBPs sequestered by cytoplasmic TDP-35 inclusions. (A) Identification of endogenous TIA1 by immunofluorescence imaging. (B) Identification of endogenous PABPC1. HEK 293T cells expressing FLAG vector, FLAG-TDP-35 or FLAG-TDP-35-4FL were imaged, showing that endogenous TIA1 (A) or PABPC1 (B) colocalized with the cytoplasmic TDP-35 inclusions. TDP-35 and its mutant were stained with anti-FLAG antibody (green), TIA1 or PABPC1 was stained with anti-TIA1 or anti-PABP antibody (red), and the nuclei were stained with Hoechst (blue). Images are representative of five experiments. Scale bars: 10 µm. The graph shown in A is the percentage of nuclear TIA1 in the cells with TDP-35 inclusions. The amounts of nuclear and total TIA1 were obtained from the pixel intensities of individual cell image and the percentage of nuclear TIA1 was calculated. The data were statistically analyzed by one-way ANOVA followed by Bonferroni post-hoc test and presented as means ±s.e.m. (Vector, n=17; TDP-35, n=18; TDP-35-4FL, n=18). *P<0.05, ****P<0.0001. (C) Supernatant–pellet fractionation for characterizing the sequestration of endogenous TIA1 into TDP-35 aggregates. HEK 293T cells were transfected with each indicated plasmid and the cell lysates were subjected to supernatant–pellet fractionation and western blotting analysis for TIA1. The proteins were detected by using anti-FLAG, anti-TIA1 and anti-actin antibodies. The two main bands indicate different isoforms of endogenous TIA1. Sup., supernatant; Pel., pellet. (D) Quantification of the amounts of TIA1 in supernatant and pellet fractions. The protein amounts were estimated from the grayscale values by using Scion Image and the data were statistically analyzed by one-way ANOVA followed by Bonferroni post-hoc test. Data are shown as means±s.e.m. (n=3). *P<0.05; ***P<0.001; N.S., not significant.

Journal of Cell Science (2022) 135, jcs259380. doi:10.1242/jcs.259380

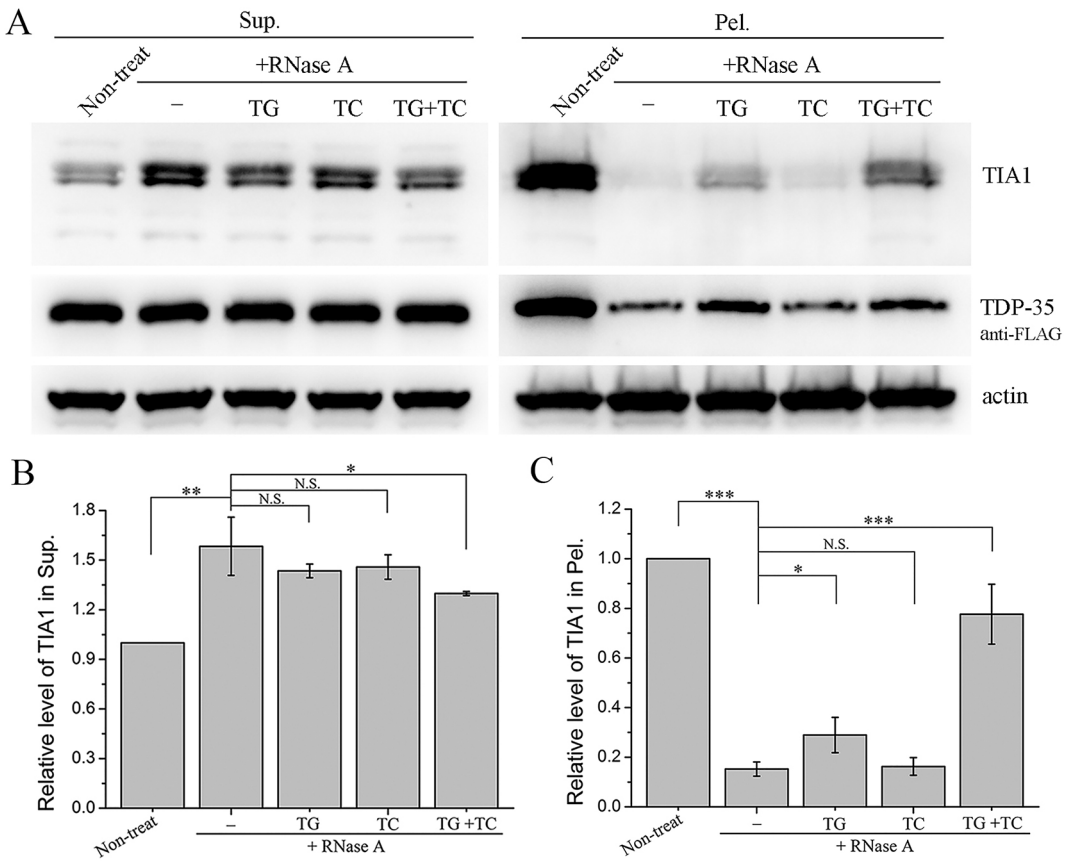

Fig. 2. RNase and ssDNA treatments showing specific RNAs involved in sequestration of TIA1 by the TDP-35 aggregates. (A) Supernatant–pellet fractionation for characterizing the effects of RNase and ssDNA treatments on the sequestration of endogenous TIA1. HEK 293T cells were transfected with the FLAG-TDP-35 plasmid, and then the cell lysates were subjected to RNase and ssDNA (~5 µM) treatments, supernatant–pellet fractionation and western blotting analysis. Non-treat, without RNase treatment; TG, TG-repeat ssDNA specifically binding to TDP-35; TC, TC-rich ssDNA specifically binding to TIA1; TG+TC, TG+TC chimera ssDNA binding with both TDP-35 and TIA1. Sup., supernatant; Pel., pellet. (B,C) Quantification of the protein amounts in supernatant (B) and pellet (C) fractions. The protein amounts were estimated from the grayscale values by using Scion Image and the data were statistically analyzed by one-way ANOVA followed by Bonferroni post-hoc test. Data are shown as means±s.e.m. (n=3). *P<0.05; **P<0.01; ***P<0.001; N.S., not significant.

To further demonstrate the role of RNAs of specific sequences in sequestration of TIA1 by TDP-35, we performed immunoprecipitation (IP) experiments with co-transfected FLAG–TDP-35 and HA–TIA1 in HEK 293T cells (Fig. 3). As expected, in the absence of RNase A, a weak TIA1 band was observed in the gel, indicating that TDP-35 associates with TIA1 in cells. When the cell lysates were subjected to RNase treatment, the TIA1 band was fully disappeared, but it was recovered by adding with the TG+TC ssDNA (Fig. 3A). As a control, association of TDP-35-4FL with TIA1 was undetectable under the same conditions (Fig. 3B), even it could not be rescued upon treatments with RNase A plus ssDNA (Fig. 3C). Similarly, TDP-35 could also immunoprecipitate with endogenous TIA1, and this precipitation effect was influenced by RNase A and/or ssDNA treatment or TDP-35-4FL mutation (Fig. S4). These data indicate that TDP-35 associates with TIA1 with the assistance of RNAs of specific sequences. In other words, TDP-35 interacts with TIA1 or other RBPs indirectly, and specific RNAs play an important role in mediating their association and sequestration.

Combined fluorescent *in situ* hybridization and immunofluorescence experiments reveal RNA-assisted sequestration

To define the role of specific RNA sequences in sequestration, we performed combined fluorescent *in situ* hybridization (FISH) and immunofluorescence experiments in HeLa cells. Different types of RNA were detected with specific Cy5-labeled probes. In the cells overexpressing TDP-35, the poly(A)-containing RNA detected with Cy5-labeled oligo-dT probe and the sequestered endogenous TIA1 were colocalized with the inclusions formed by TDP-35 in the cytoplasm (Fig. 4A), indicating that this type of RNA (especially mRNA) plays a role in mediating TDP-35 and TIA1 (as well as TDP-43; Che et al., 2015) to form cytoplasmic inclusions. Moreover, the specific UG-rich RNAs detected with a Cy5–CA probe not only largely dispersed in the nucleus but also accumulated in condensate puncta in the cytoplasm, wherein the UG-rich RNAs and the sequestered TIA1 were colocalized with the TDP-35 inclusions (Fig. 4B). As a negative control, the random sequence RNAs detected with a Cy5–NN probe exhibited a different distribution pattern in the cytoplasm and were not colocalized with TDP-35 and TIA1 in the inclusions (Fig. 4C). Similar observations were also obtained in HEK 293T cells (Fig. S5), suggesting that TDP-35 sequesters TIA1 into cytoplasmic inclusions through RNAs of specific sequences. Thus, we propose that RNAs (mRNAs) containing UG- and UC-rich sequences mediate the association of TDP-35 with TIA1, leading to sequestration of endogenous TIA1 by the cytoplasmic TDP-35 inclusions.

Sequestration of TIA1 by TDP-35 leads to reduction of the expression level of PRKRA

According to our hijacking hypothesis, protein aggregates can sequester cellular interacting partners, leading to cellular

Journal of Cell Science (2022) 135, jcs259380. doi:10.1242/jcs.259380

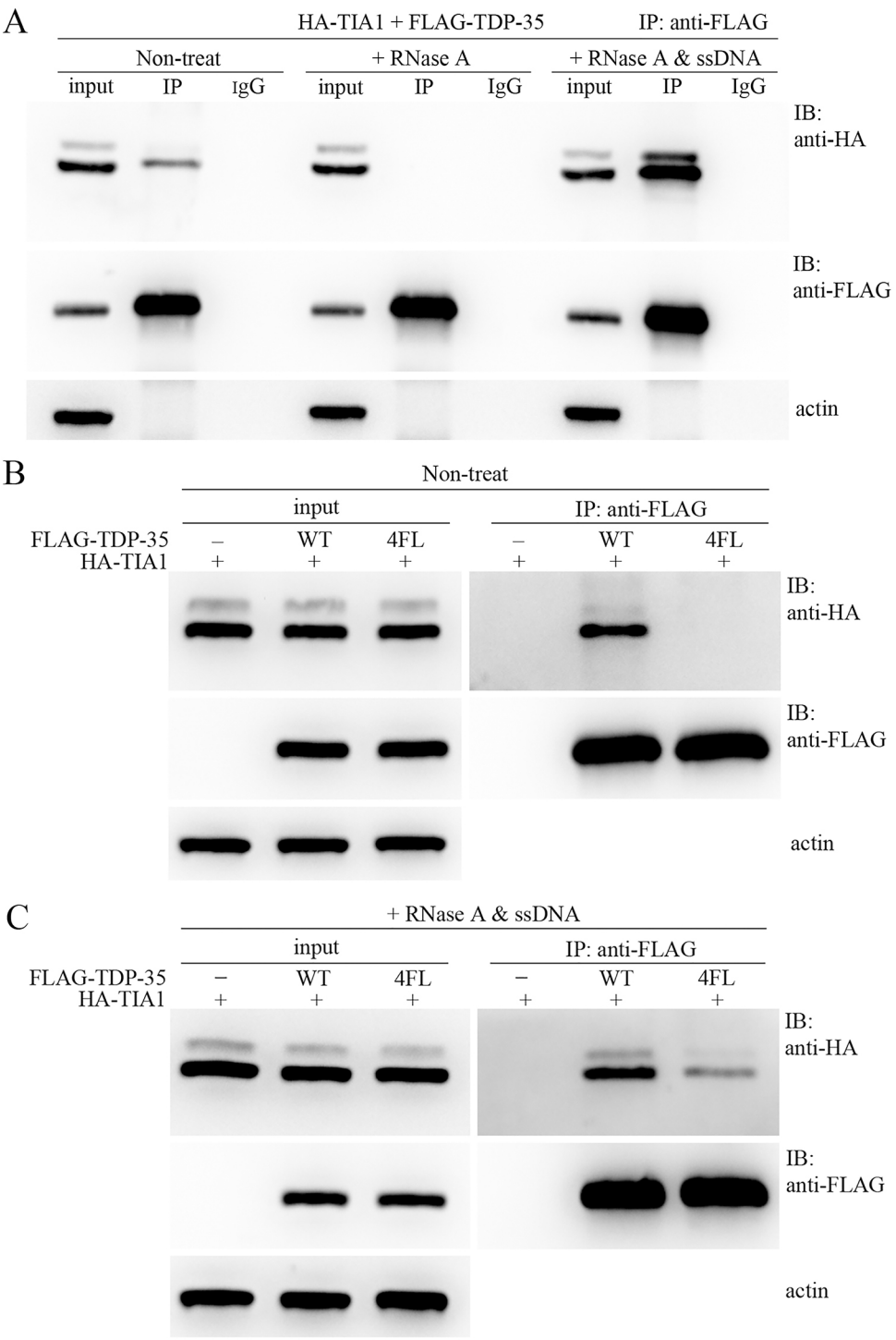

Fig. 3. TDP-35 associates with TIA1 mediated by sequence-specific RNA. (A) Co-immunoprecipitation (co-IP) experiment examining the effects of RNase and ssDNA treatments on the association of FLAG-TDP-35 with HA-TIA1. The supernatants were immunoprecipitated (IP) with protein A/G beads plus FLAG antibody under various conditions including no treatment (non-treat), after RNase treatment, and RNase A plus TG+TC ssDNA treatment. IgG, a control without FLAG antibody; IP, with anti-FLAG antibody. The immunoblotting was carried out with an antibody against either HA or FLAG. ssDNA, single-stranded DNA (TG+TC). (B) Co-IP for association of FLAG–TDP-35 or its FLAG–TDP-35-4FL mutant with HA–TIA1. The co-IP was under the condition of no treatment. (C) Co-IP for ssDNA-assisted association of FLAG–TDP-35 with HA–TIA1. FLAG–TDP-35-4FL was set as a control. All the co-IP experiments were under the condition of RNase and/or TG+TC ssDNA (~2.5 µM) treatment. In all co-IP experiments, ~8% loading of the sample was applied for input. Images shown are representative of three experiments.

dysfunctions and cytotoxicities of the hijacked partners (Yang and Hu, 2016; Yang et al., 2014). As TIA1 and TIAR (also known as TIAL1) proteins are essential for accurate processing of the interferon-inducible double-stranded RNA-dependent protein kinase activator A (PRKRA) mRNA (Patel and Sen, 1998), and thus might regulate the protein level of PRKRA (Meyer et al., 2018), we investigated the effect of TIA1 and/or TIAR sequestration on the expression levels of PRKRA in HEK 293T cells. Firstly, we performed a semi-quantative RT-PCR experiment to examine the effect of TDP-35 overexpression on the alternative splicing of *PRKRA* mRNA. As expected from the literature, there were three spliced isoforms identified in the gel (Fig. 5A), for which it is the mature form (isoform I) that can translate into the PRKRA protein (Meyer et al., 2018). Compared with the vector control, overexpression of TDP-35 attenuated the abundance of the major form (isoform I) as well as total *PRKRA* mRNA (Fig. 5A), whereas TDP-35-4FL had little effect on them. This indicates that sequestration of TIA1 and/or TIAR influences their splicing of *PRKRA* mRNA and its mRNA stability (Meyer et al., 2018). Secondly, on the protein level, overexpression of TDP-35 significantly reduced the PRKRA level (Fig. 5B), whereas that of TDP-35-4FL had little effect on the protein level. Moreover, the

Journal of Cell Science (2022) 135, jcs259380. doi:10.1242/jcs.259380

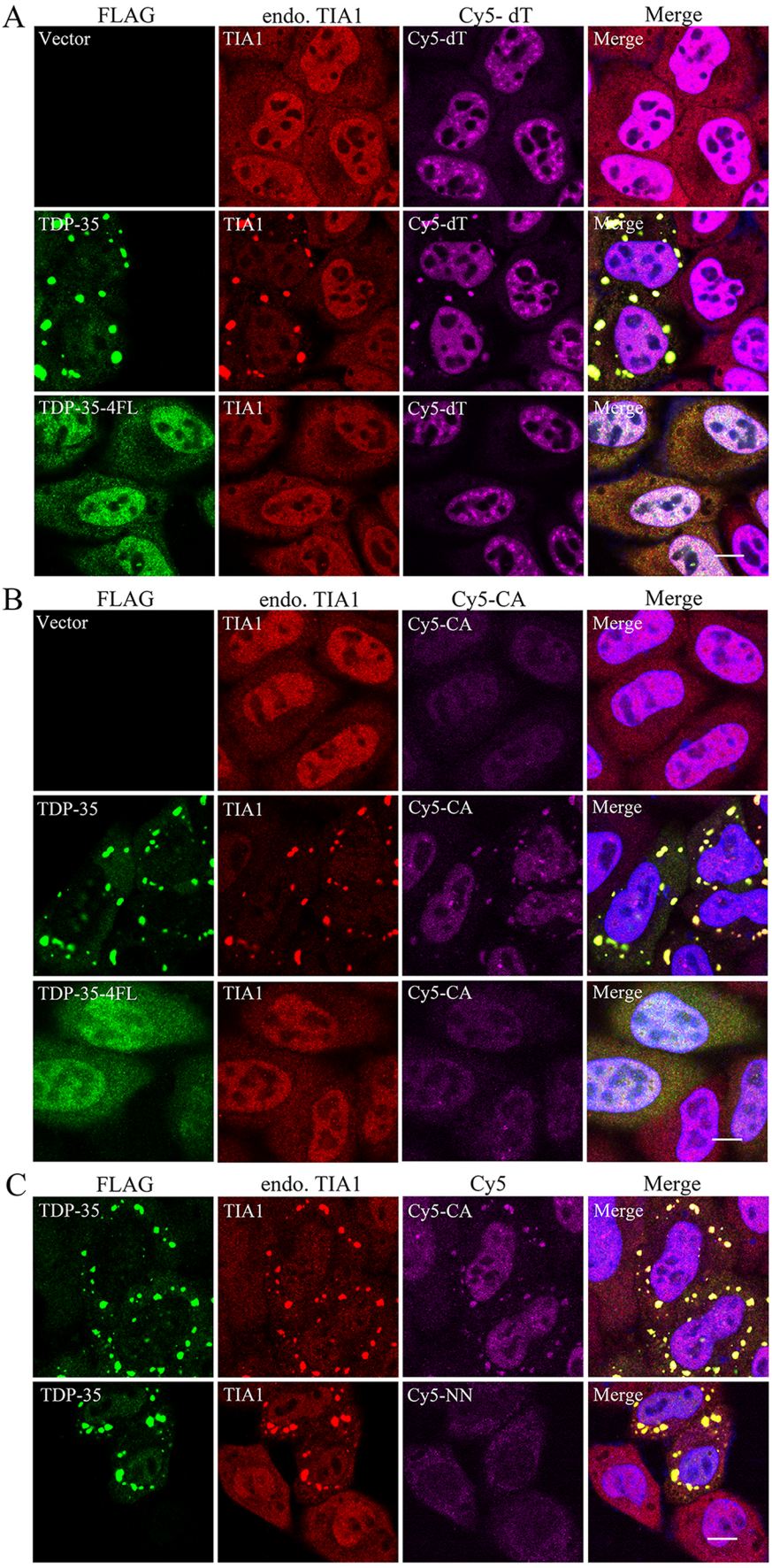

Fig. 4. Combined FISH and immunofluorescence experiment for detecting specific RNAs enriched in the TDP-35 inclusions in HeLa cells. (A) Microscopy imaging with the Cy5-oligo-dT probe showing poly(A)-containing RNAs enriched in the cytoplasmic TDP-35 inclusions and colocalized with endogenous TIA1. (B) Imaging with the Cy5–CA probe showing UG-repeat RNAs in the inclusions. (C) Imaging with the Cy5–NN probe for random RNAs as a negative control. FLAG–TDP-35 and FLAG–TDP-35-4FL are in green, TIA1 is in red, RNAs are in pink, while the nuclei are in blue (Hoechst). Images shown are representative of three experiments. Scale bars: 10 µm.

Journal of Cell Science (2022) 135, jcs259380. doi:10.1242/jcs.259380

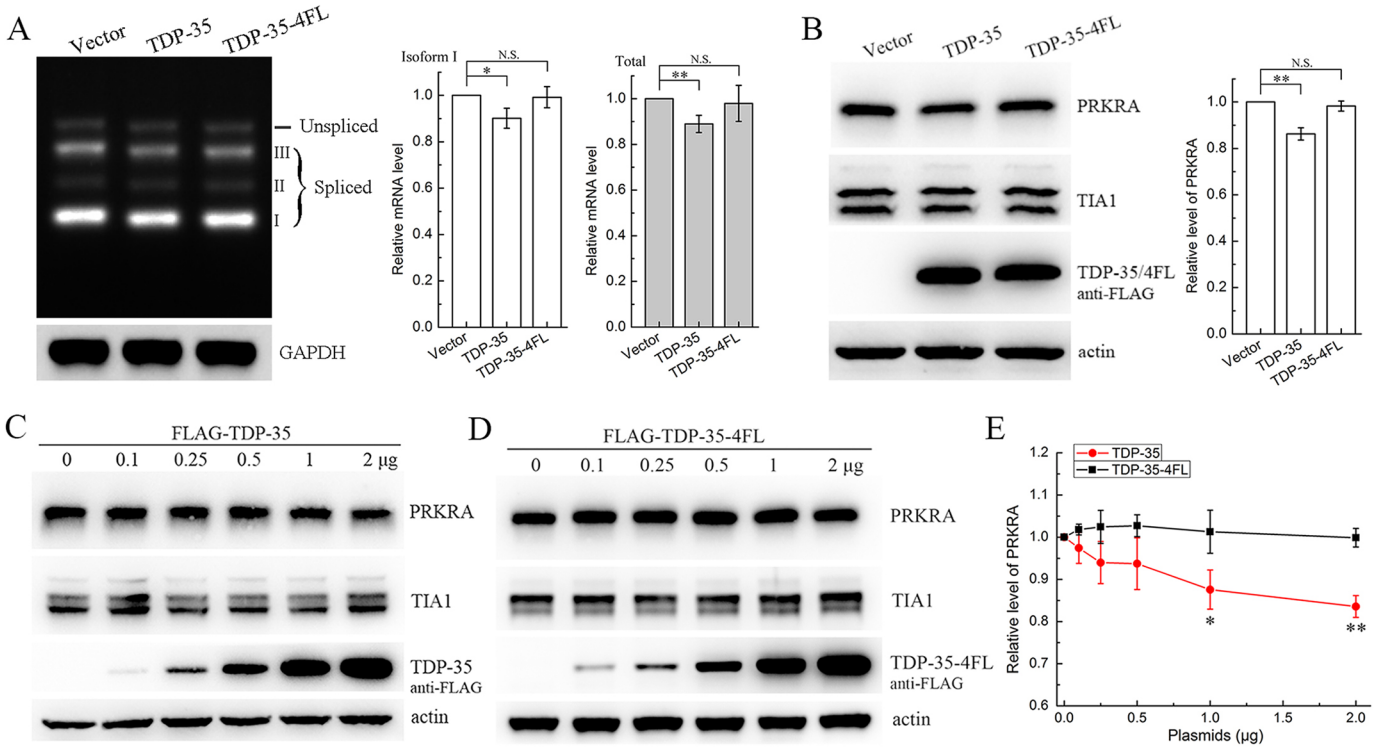

Fig. 5. Formation of the TDP-35 inclusions influences the expression level of RPKRA in HEK 293T cells. (A) Effect of TDP-35 overexpression on the alternative splicing of *PRKRA* mRNA. TDP-35-4FL was set as a control. The upper band is the unspliced mRNA of *PRKRA*, whereas the lower three bands for spliced mRNA of isoform I, II and III, respectively. The intensity of the mature spliced mRNA (isoform I) was quantified in each condition and normalized with that of GAPDH, with the total mRNA being the sum of unspliced and three spliced isoforms. (B) Effect of TDP-35 overexpression on the protein level of RPKRA. HEK 293T cells were transfected with each indicated plasmid, the cell lysates were centrifuged, and then the supernatant was subjected to western blotting analysis. (C) Dose-dependent experiment for alteration of the RPKRA level upon overexpression of TDP-35. (D) As in C, but upon overexpression of TDP-35-4FL. (E) Quantification of the PRKRA levels upon over-expression of TDP-35 or TDP-35-4FL as in C,D. Data are shown as means±s.e.m. (n=3). *P<0.05; **P<0.01; N.S., not significant.

reduction of PRKRA caused by TDP-35 overexpression was dependent on the TDP-35 level (Fig. 5C,E), whereas that did not occur with an increased dose of the mutant (Fig. 5D,E). Similarly, this downregulation effect was also observed in a dose-dependent manner in HeLa cells (Fig. S6). Collectively, these data demonstrate that TDP-35 overexpression downregulates the expression level of PRKRA and imply that this deregulation is caused by sequestration of TIA1 and probably TIAR. Therefore, TDP-35 sequesters TIA1 and/or TIAR into cytoplasmic inclusions, leading to dysfunction of TIA1 and/or TIAR that ultimately impairs the downstream expression.

Live-cell imaging authenticates the sequestration of TDP-43 by cytoplasmic TDP-35 inclusions

Our previous study demonstrated that the cytoplasmic inclusions formed by TDP-35 sequester full-length TDP-43 via poly(A)-containing RNA (Che et al., 2015), but most of the data were obtained from averaging multiple cultured cells. To animate the process by which TDP-35 sequesters endogenous TDP-43 into cytoplasmic inclusions, we engineered a HEK 293T cell line stably expressing endogenous EGFP-tagged TDP-43 protein through CRISPR/Cas9 techniques, and performed fluorescence microscopy imaging in living cells. We firstly examined whether the TDP-35 inclusions can sequester endogenous EGFP–TDP-43 protein. FLAG–TDP-35 was transiently expressed in the EGFP–TDP-43 cell line, and after transfection, the TDP-35 inclusions were visualized by using an anti-FLAG antibody and TDP-43 was directly observed via its GFP fluorescence at different time points. As shown in Fig. 6A, in the cells expressing TDP-35 puncta were formed and TDP-43 was observed present in the cytoplasmic inclusions, whereas in the cells without TDP-35 expression, TDP-43 retained its nuclear distribution. This suggests that a population of endogenous TDP-43 was mis-localized in the cytoplasm and especially it might be driven into the TDP-35 inclusions. More importantly, within 18 h after transfection, expression of TDP-35 was sufficient to sequester endogenous TDP-43, and the sequestration and colocalization became more efficient with longer culture time. Next, we directly visualized the TDP-43 molecules being transported into the cytoplasmic TDP-35 inclusions in living cells. The images showed that TDP-43 firstly re-distributed from nucleus into the cytoplasm and then appeared gradually in the large round puncta (Fig. 6B; Movie 1). This implies that endogenous TDP-43 is able to be sequestered into the cytoplasmic inclusions from nucleus distribution even though TDP-35 is unobservable in this experiment.

From the above experiments, we have seen TDP-43 is sequestered from the nucleus to the cytoplasm in living cells, but whether this is triggered by the TDP-35 inclusions or cell stress remained obscure. To resolve this point, we next generated two mCherry-tagged TDP-35 constructs, but found only the C-terminally tagged TDP-35-mCherry formed cytoplasmic inclusions in HEK 293T cells. The TDP-35–mCherry plasmid was transiently transfected into the EGFP–TDP-43 cell line, and ∼12 h later, live-cell imaging was started to monitor the dynamic events of endogenous TDP-43. Consistent with our above

Journal of Cell Science (2022) 135, jcs259380. doi:10.1242/jcs.259380

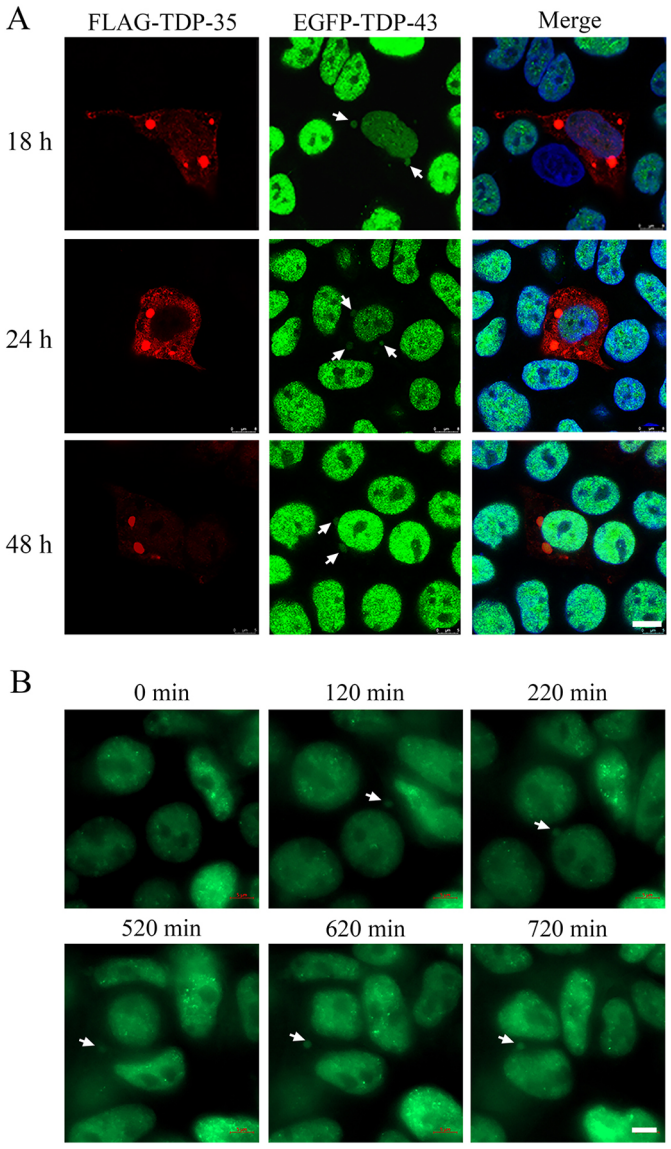

Fig. 6. Fluorescence microscopic imaging for sequestration of TDP-43 in the EGFP-TDP-43 cell line. (A) Colocalization of TDP-43 with the TDP-35 inclusions. Representative images for the immunofluorescence analysis of FLAG–TDP-35 in the EGFP–TDP-43 HEK 293T cell line are shown. The images were recorded at 18, 24 and 48 h after expression of FLAG–TDP-35. TDP-35 was stained with anti-FLAG antibody (red), TDP-43 was indicated from the fluorescence of its fused EGFP (green), and nuclei were stained with Hoechst (blue). Scale bar: 10 µm. (B) Live-cell imaging. Excerpts from a time-lapse movie imaged with 20-min intervals in the EGFP–TDP-43 cell line transfected with FLAG–TDP-35. The imaging began at ∼12 h after transfection with FLAG–TDP-35. Scale bar: 5 µm. The cytoplasmic inclusions colocalized with EGFP–TDP-43 are indicated with arrows. Images shown are representative of four experiments.

observations, TDP-35–mCherry firstly formed cytoplasmic inclusions, and a population of TDP-43 was mis-localized into the cytoplasm and colocalized with the cytoplasmic TDP-35 inclusions (Fig. 7A; Movie 2). Interestingly, we observed an accumulation of EGFP fluorescence signal in the TDP-35 inclusions with a lag time, suggesting that the TDP-35 inclusions sequester endogenous TDP-43 and this event occurs after formation of the TDP-35 inclusions. Quantification of the fluorescence intensities of mCherry and EGFP for each punctum also revealed that the cytoplasmic fraction of TDP-43 that colocalized with the

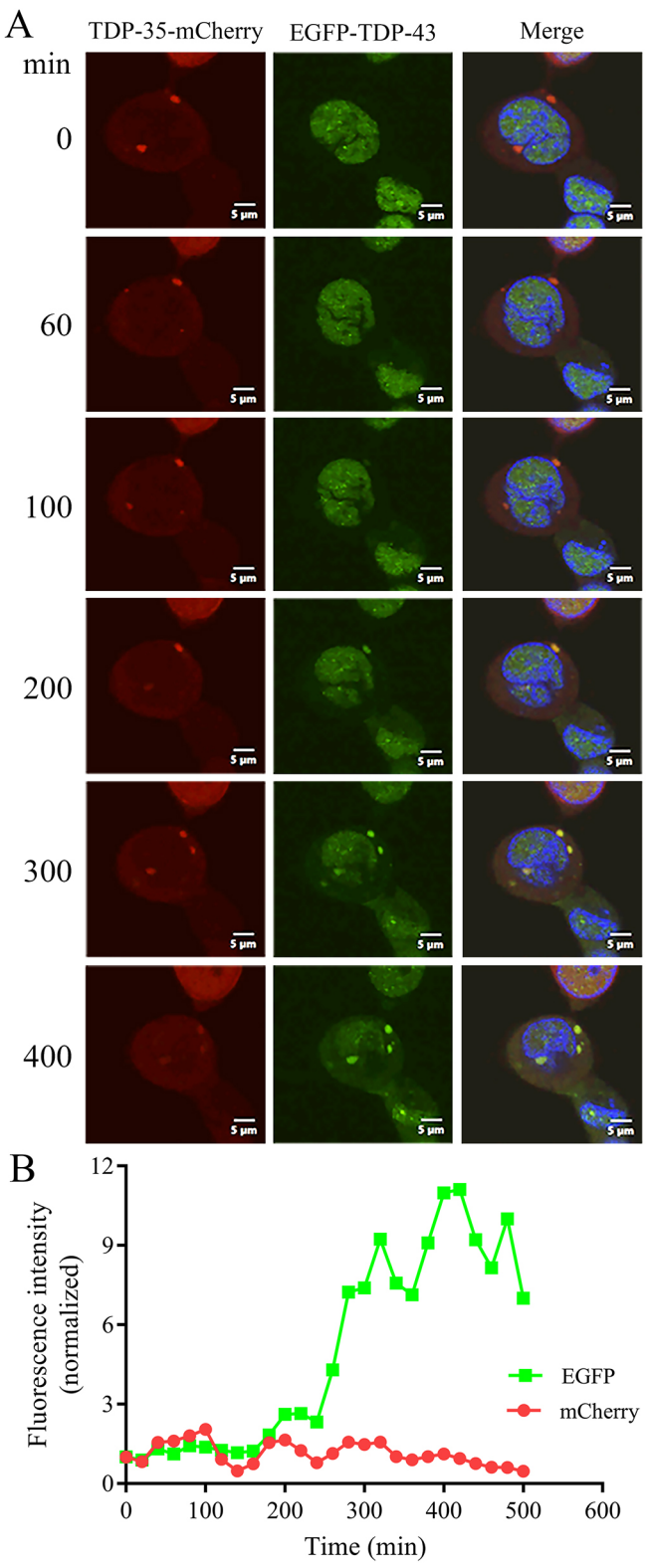

Fig. 7. Live-cell imaging for sequestration of TDP-43 by the TDP-35 inclusions. (A) Excerpts from a time-lapse movie imaged with 20-min intervals in the EGFP–TDP-43 HEK 293T cell line transfected with TDP-35–mCherry. The imaging began at ∼12 h after transfection with TDP-35–mCherry. Scale bars: 5 µm. The images are aligned starting at the 0-min time point based on appearance of the EGFP–TDP-43 signals in the TDP-35 inclusions. Images shown are representative of four experiments. (B) Quantification of the fluorescence intensities of mCherry and EGFP for a representative inclusion in a time-lapse movie. The intensity data are normalized to that of the 0-min point.

Journal of Cell Science (2022) 135, jcs259380. doi:10.1242/jcs.259380

TDP-35 inclusions was progressively increased, but the mCherry signal remained almost constant over time (Fig. 7B; Fig. S7). This strongly suggests that the TDP-35 inclusions trigger the endogenous TDP-43 molecules to escape from the nucleus where they become sequestered into the cytoplasmic inclusions.

DISCUSSION

Our previous studies have revealed that TDP-35, a C-terminal fragment of TDP-43, forms cytoplasmic inclusions and sequesters full-length TDP-43 into the inclusions (Che et al., 2015), which was proposed to be associated with the TDP-43 proteinopathy. In this research, we demonstrate the dynamic sequestration process, showing that formation of the cytoplasmic TDP-35 inclusions precedes sequestration of the full-length TDP-43. The nucleus-localized TDP-43 re-distributes into the cytoplasmic inclusions formed by its C-terminal fragment TDP-35. To our knowledge, this is for the first time that the dynamic process of sequestration triggered by protein aggregates or inclusions in living cells has been directly visualized, and exemplifies that a truncated form sequesters its full-length protein into the inclusions. This dynamic imaging provides direct and solid evidence in support of our hijacking model where sequestration of cellular interacting partners by protein aggregates or inclusions is implicated in a pathological mechanism of proteinopathies (Yang and Hu, 2016; Yang et al., 2014).

TDP-43 is an RBP with two RRM domains, and its C-terminal fragment TDP-35 still retains its RNA-binding ability (Che et al., 2015). Mutation in the RRM domains might destroy its RNA-binding ability and cause functional loss of the protein (Buratti and Baralle, 2001). Mann et al. reported that the RNA-bound TDP-43 phase separates into SGs, but the RNA-free form experiences aberrant phase transition to TDP-43 proteinopathy (Mann et al., 2019). Interestingly, oligonucleotide RNA antagonizes the neurotoxic phase transition of TDP-43. We presume that specific RNA sequences play critical roles in mediating the sequestration of TIA1 and other RBPs. For example, TDP-43 and TDP-35 specifically binds with UG-repeat RNA sequences (Lukavsky et al., 2013; Passoni et al., 2012), whereas TIA1 binds to UC-rich sequences (Waris et al., 2017). Our experiments with ssDNA and FISH probes strongly demonstrate that these specific sequences (UG repeats for TDP-35 and UC-rich for TIA1) are important for the formation of the cytoplasmic TDP-35 inclusions and sequestration of TIA1. By using the oligo-dT probe, these RNAs were defined to be poly(A)-containing RNA (especially mRNA), while the CA probe indicated that this type of RNA contained UG-rich sequences. Thus, we conclude that TDP-35 associates with other RBPs and sequesters them into cytoplasmic inclusions in an RNA-dependent manner. We propose that the RNA-assisted sequestration plays important roles in protein association, inclusion formation and even co-pathologies for the diverse RBPs. Of note, there is still little evidence demonstrating that specific RNAs localize in the TDP-43 inclusions in human post-mortem material; one possible reason is that TDP-43 deposition leads to destabilization of the targeted RNA in ALS/FTLD (Tank et al., 2018), another is the technical challenge in charactering RNA foci in brain tissue (Highet et al., 2021; Mehta et al., 2020). The specific RNA molecules that assist sequestration of TDP-43 and other RBPs by TDP-35 in cells and even brain tissue remains to be characterized.

The TIA proteins are commonly localized in SGs and are supposed to be involved in the granule formation (Mackenzie et al., 2017; Waris et al., 2014). TIA1 is often stated to be a molecular marker for RNA granules, but whether its sequestration is associated with the formation of these SGs remains unclear. We propose that the cytoplasmic TDP-35 inclusions (aggregates) are more condensed than the TIA1-positive SGs; their dynamic behaviors, sequestration kinetics and even the cellular impacts are also different. Hence, sequestration of TIA1 into the TDP-35 inclusions (aggregates) might interfere with the formation of SGs upon heat or arsenite treatment. TIA1 commonly distributes mainly in the nucleus while also being dispersed in the cytoplasm (Kedersha et al., 1999), and sequestration by TDP-35 may re-locate it into the cytoplasmic inclusions and accordingly reduce its nuclear abundance. The normal function of TIA1 is in regulating the pre-mRNA processing of PRKRA and thus its protein level (Meyer et al., 2018). Our data suggest that the sequestration of TIA1 by TDP-35 results in dysregulation of TIA1 and alteration of the expression level of PRKRA. This functional deregulation may be one of the fundamental elements in TDP-43–TDP-35 proteinopathies.

TDP-43 is a pathological marker for ALS and FTLD, and it might co-aggregate with other pathogenic proteins. The ALS-linked mutations of TIA1 promote its phase separation and alter the SG dynamics, in which the recruited TDP-43 becomes immobile and insoluble (Mackenzie et al., 2017). Recently, Lee et al. reported that arsenite induces sequestration of cytoplasmic TDP-43 into TIA1-positive SGs (Lee et al., 2021). In addition, TDP-43 has also been reported to co-occur with other RBPs including G3BP1 (Aulas et al., 2015), Matr3 (Johnson et al., 2014), Atx2 (Elden et al., 2010; Toyoshima et al., 2011) and hnRNPs (Kim et al., 2013). Association or co-aggregation of TDP-43 with these RBPs contributes to SG formation and the co-pathologies of ALS, FTLD and other NDs. We have confirmed that hnRNPA2/B1 is colocalized in the cytoplasmic TDP-35 inclusions, but neither Matr3 nor hnRNP A1 were identified in the inclusions under our experimental conditions. Interestingly, the cytoplasmic form of PABP (PABPC1) but not its nuclear form PABPN1 colocalized with the cytoplasmic TDP-35 inclusions. Considering the fact that the nucleus-addressed TDP-43 can be sequestered by TDP-35, the selective colocalization of RBPs in the TDP-35 inclusions might be attributable to their RNA-binding specificities. Thus, we propose that the cytoplasmic TDP-35 inclusions associate with, and sequester, TDP-43 and other specific RBPs, and co-aggregation of these pathologically amyloidogenic RBPs potentially contributes to the co-pathologies of ALS, FTLD and other NDs.

MATERIALS AND METHODS

Plasmids, antibodies, and reagents

The cDNAs for encoding TDP-35 (residues 90–414) and its mutant (TDP-35-4FL, which has mutations F147L, F149L, F229L and F231L) were cloned into the FLAG-pcDNA3.1 vector), and the cDNA for N- or C-terminally mCherry-tagged TDP-35 was cloned into the FLAG-pcDNA3.1 or pcDNA3.1-FLAG vector. The cDNAs for encoding TIA1 and PABPC1 were cloned into the HA–pcDNA3.0 vector. The cloning vectors were from in-house stocks. All constructs were validated by DNA sequencing as listed in Table S1. All primary antibodies used in this study are listed in Table S2. The secondary antibodies were from Jackson ImmunoResearch Laboratories.

Cell culture, transfection and western blotting analysis

HEK 293T cells and HeLa cells (Cell Bank of Chinese Academy of Sciences) were cultured in Dulbecco's modified Eagle's medium (DMEM; HyClone) supplemented with 10% fetal bovine serum (Gemini) and penicillin-streptomycin at 37°C under a humidified atmosphere containing 5% CO_2. The cell lines were checked for mycoplasma contamination at regular intervals. All transfections of plasmids were performed by using

PolyJet™ reagent (SignaGen) following the manufacturer's instructions. Protein samples of lysates or fractions were subjected to SDS-PAGE and transferred onto PVDF membranes (PerkinElmer or Millipore). When needed, the blots were cut prior to antibody hybridization. The indicated proteins were detected with specific primary and secondary antibodies and detected by an ECL detection kit (Thermo Fisher Scientific). For quantification, the integral grayscale values of protein bands were recorded by using Scion Image software.

Supernatant–pellet fractionation

About 48 h after transfection, the HEK 293T or HeLa cells were harvested and lysed in 100 µl of a RIPA buffer [50 mM Tris-HCl pH 7.5, 150 mM NaCl, 1 mM EDTA, 1% Nonidet P-40, and cocktail protease inhibitor (Roche)] on ice for 30 min, and then centrifuged at 13,800 ***g*** for 15 min at 4°C. The supernatant was added with 100 µl of 2× loading buffer (2% SDS), while the pellet was sufficiently washed with the RIPA buffer three times at 4°C and then 50 µl of 4× loading buffer (4% SDS) was added. Equal volumes of the supernatant and pellet fractions were subjected to SDS-PAGE and western blotting analysis. RNase A (Invitrogen) and/or plus ssDNA (Sangon) were added when the cells were subjected to lysis. The final concentration of ssDNA was ∼5 µM and that of RNase A was 0.5 mg/ml. The ssDNA sequences are shown in Table S3.

Immunofluorescence microscopy and immunoprecipitation

For immunofluorescence microscopy, ∼24 h after transfection, HEK 293T or HeLa cells grown on glass coverslips were washed with PBS buffer (10 mM Na_2HPO_4, 1.8 mM KH_2PO_4, 140 mM NaCl, 2.7 mM KCl, pH 7.3) and fixed with 4% paraformaldehyde for 15 min, permeabilized with 0.1% Triton X-100, and blocked with blocking solution (5% BSA and 10% FBS in PBS buffer) for 1 h at room temperature. Then the fixed cells were incubated with the respective primary antibodies overnight at 4°C. After washing with the PBS buffer, the cells were incubated with an FITC-conjugated antibody and a TRITC-conjugated antibody (Jackson ImmunoResearch Laboratories). The nuclei were stained with Hoechst 33342 (Sigma). The cells were visualized on a Leica TCS SP8 confocal microscope (Leica Microsystems).

For the immunoprecipitation assay, the HEK 293T cells were harvested at 48 h post-transfection and lysed in PEB buffer [10 mM HEPES, pH 7.4, 100 mM KCl, 5 mM $MgCl_2$, 1 mM DTT, 0.1% Nonidet P-40, 1 mM PMSF, supplemented with cocktail protease inhibitor (Roche)] on ice for 30 min, and then centrifuged at 13,800 ***g*** for 20 min at 4°C. Protein A/G plus agarose (Santa Cruz Biotechnology) was washed and incubated with mouse anti-FLAG antibody (1:1000; F1804, Sigma) for ∼1 h at 4°C, and then the supernatant was added and further incubated for another 4 h at 4°C, meanwhile, the control was incubated with protein A/G Agarose beads and mouse IgG antibody. The beads were washed with the PEB buffer for three times and boiled in 50 µl of 2× sampleloading buffer. Then the proteins were analyzed by immunoblotting. Similar experiments with RNase and/or plus ssDNA treatments were also performed; the RNase A and/or ssDNA were added during the incubation with the supernatant. The chimera TG+TC ssDNA (∼2.5 µM) was used in this experiment.

Combined FISH and immunofluorescence

The method for preparing samples for imaging RNA/protein was as described previously (Che et al., 2015). Briefly, HeLa or HEK 293T cells on glass coverslips were washed with 1× PBS and fixed with 4% paraformaldehyde for 15 min and permeabilized with 0.1% Triton X-100 for 15 min, and then washed with 2× SSC (Sangon) for 10 min at room temperature. The cells were hybridized with the FISH probes overnight at 42°C. Then the cells were washed continuously two times with 2×SSC, 0.5× SSC and 1× PBS in dark at room temperature. Immunofluorescence was performed by incubating the fixed cells with the primary antibodies in blocking buffer (2% BSA in 1× PBS) for 1 h at room temperature. The cells were then washed three times with 1× PBS for 5 min each and incubated with the secondary antibody and Hoechst 33342 in blocking buffer for another 1 h at room temperature. The immunofluorescence experiment was carried out under the condition of light protection. The FISH probes were synthesized and labeled with Cy5 at the 5′ end (Sangon), and their sequences are shown in Table S3.

RNA isolation, cDNA synthesis and alternative splicing analysis

The alternative splicing events of *PRKRA* mRNA were detected as described previously (Meyer et al., 2018). HEK 293T cells were transfected with the FLAG-tagged plasmids respectively and harvested at∼48 h after transfection. Total RNA was isolated using TRIzol Reagent (Thermo Fisher-Invitrogen). According to the manufacturer's instructions, the cDNAs were synthesized with Hifair® III 1st Strand cDNA Synthesis kit (gDNA digester plus) (Yeasen Biotech) using oligo$(dT)_{18}$ primer and 1 µg of total RNA. Total 20 µl of the cDNA product was diluted to 100 µl, then 5 µl of the diluted cDNA was used for subsequent PCR amplification. PCR amplification was performed using 2×Taq PCR MasterMix (Tiangen Biotech) in a 25-µl reaction solution, containing 12.5 µl of PCR MasterMix, 5 µl of the diluted cDNA template and 0.5 mM of each primer. GAPDH was chosen as the loading control. The primers used for PCR are listed in Table S3. Three independent experiments were performed. The intensity of spliced band was quantified by Scion Image software (Scion Corp) and the spliced levels of *PRKRA* mRNA were compared.

Live-cell imaging and imaging processing

For live-cell imaging, we first generated a cell line on HEK 293T cells stably expressing EGFP-tagged TDP-43 by using CRISPR/Cas9 techniques as described in our previous work (Xue et al., 2020a). The EGFP–TDP-43 cells were plated on a 29-mm dish with 20-mm glass-bottom wells (Cellvis). At ∼12 h after transfection with FLAG–TDP-35 or TDP-35–mCherry, the growth medium was replaced with fresh medium containing 0.2 mg/ml Hoechst 33342 (Sigma) to stain the nuclei. The cells were then imaged on an inverted laser scanning confocal microscope, Zeiss Celldiscoverer 7 (Zeiss) or Olympus SpinSR (Olympus) at 20-min intervals. During imaging, the cells were kept at 37°C and under a chamber with 5% CO_2. For processing of the live-cell images, the fluorescence intensities of individual inclusions were recorded by using the CellSens imaging software (Olympus) beginning at the time point of EGFP–TDP-43 inclusion formation. The intensity value of each time point was normalized to that of the starting point. The intensity profiles for individual inclusions were plotted with GraphPad Prism software.

Statistical analysis

Data from at least three independent experiments were obtained from the integral grayscale values of indicated protein bands in western blots and normalized to that of the respective control. Then the relative levels for protein amounts were presented as means±s.e.m. Statistical analyses were performed with one-way ANOVA program followed by Bonferroni post-hoc test, and the quantitative data were presented by using OriginPro software. Differences were considered statistically significant at $P<0.05$. In all experiments, the *P*-values were labeled in the graphs as $*P<0.05$, $**P<0.01$, $***P<0.001$, $****P<0.0001$ or N.S. (not significant).

Acknowledgements

The authors would thank the Core Facility for Cell Biology at SIBCB, CAS for providing technical support in microscopic imaging.

Competing interests

The authors declare no competing or financial interests.

Author contributions

Conceptualization: H-Y.H.; Methodology: W.-L.G., S.-X.Z.; Investigation: L.-L.J., W.-L.G., J.-Y.W., S.-X.Z.; Resources: L.-L.J.; Writing - original draft: L.-L.J., W.-L.G.; Writing - review & editing: H-Y.H.

Funding

This work was supported by grants from the National Natural Science Foundation of China (31670782, 31700669 and 31870764).

Peer review history

The peer review history is available online at https://journals.biologists.com/jcs/article-lookup/doi/10.1242/jcs.259380.

References

Afonina, E., Stauber, R. and Pavlakis, G. N. (1998). The human poly(A)-binding protein 1 shuttles between the nucleus and the cytoplasm. *J. Biol. Chem.* **273**, 13015-13021. doi:10.1074/jbc.273.21.13015

Arai, T., Hasegawa, M., Akiyama, H., Ikeda, K., Nonaka, T., Mori, H., Mann, D., Tsuchiya, K., Yoshida, M., Hashizume, Y. et al. (2006). TDP-43 is a component of ubiquitin-positive tau-negative inclusions in frontotemporal lobar degeneration and amyotrophic lateral sclerosis. *Biochem. Biophys. Res. Commun.* **351**, 602-611. doi:10.1016/j.bbrc.2006.10.093

Aulas, A., Caron, G., Gkogkas, C. G., Mohamed, N. V., Destroismaisons, L., Sonenberg, N., Leclerc, N., Parker, J. A. and Vande Velde, C. (2015). G3BP1 promotes stress-induced RNA granule interactions to preserve polyadenylated mRNA. *J. Cell Biol.* **209**, 73-84. doi:10.1083/jcb.201408092

Ayala, Y. M., Pantano, S., D'Ambrogio, A., Buratti, E., Brindisi, A., Marchetti, C., Romano, M. and Baralle, F. E. (2005). Human, Drosophila, and C.elegans TDP43: nucleic acid binding properties and splicing regulatory function. *J. Mol. Biol.* **348**, 575-588. doi:10.1016/j.jmb.2005.02.038

Banerjee, A., Apponi, L. H., Pavlath, G. K. and Corbett, A. H. (2013). PABPN1: molecular function and muscle disease. *FEBS J.* **280**, 4230-4250. doi:10.1111/febs.12294

Besnard-Guerin, C. (2020). Cytoplasmic localization of amyotrophic lateral sclerosis-related TDP-43 proteins modulates stress granule formation. *Eur. J. Neurosci.* **52**, 3995-4008. doi:10.1111/ejn.14762

Bhardwaj, A., Myers, M. P., Buratti, E. and Baralle, F. E. (2013). Characterizing TDP-43 interaction with its RNA targets. *Nucleic Acids Res.* **41**, 5062-5074. doi:10.1093/nar/gkt189

Budini, M., Buratti, E., Stuani, C., Guarnaccia, C., Romano, V., De Conti, L. and Baralle, F. E. (2012). Cellular model of TAR DNA-binding protein 43 (TDP-43) aggregation based on its C-terminal Gln/Asn-rich region. *J. Biol. Chem.* **287**, 7512-7525. doi:10.1074/jbc.M111.288720

Buratti, E. and Baralle, F. E. (2001). Characterization and functional implications of the RNA binding properties of nuclear factor TDP-43, a novel splicing regulator of CFTR exon 9. *J. Biol. Chem.* **276**, 36337-36343. doi:10.1074/jbc.M104236200

Buratti, E. and Baralle, F. E. (2010). The multiple roles of TDP-43 in pre-mRNA processing and gene expression regulation. *RNA Biol.* **7**, 420-429. doi:10.4161/rna.7.4.12205

Buratti, E., Brindisi, A., Giombi, M., Tisminetzky, S., Ayala, Y. M. and Baralle, F. E. (2005). TDP-43 binds heterogeneous nuclear ribonucleoprotein A/B through its C-terminal tail: an important region for the inhibition of cystic fibrosis transmembrane conductance regulator exon 9 splicing. *J. Biol. Chem.* **280**, 37572-37584. doi:10.1074/jbc.M505557200

Calabretta, S. and Richard, S. (2015). Emerging Roles of Disordered Sequences in RNA-Binding Proteins. *Trends Biochem. Sci.* **40**, 662-672. doi:10.1016/j.tibs.2015.08.012

Cascella, R., Capitini, C., Fani, G., Dobson, C. M., Cecchi, C. and Chiti, F. (2016). Quantification of the Relative Contributions of Loss-of-function and Gain-of-function Mechanisms in TAR DNA-binding Protein 43 (TDP-43) Proteinopathies. *J. Biol. Chem.* **291**, 19437-19448. doi:10.1074/jbc.M116.737726

Chen, H. J. and Mitchell, J. C. (2021). Mechanisms of TDP-43 proteinopathy onset and propagation. *Int. J. Mol. Sci.* **22**, 6004. doi:10.3390/ijms22116004

Che, M. X., Jiang, Y. J., Xie, Y. Y., Jiang, L. L. and Hu, H. Y. (2011). Aggregation of the 35-kDa fragment of TDP-43 causes formation of cytoplasmic inclusions and alteration of RNA processing. *FASEB J.* **25**, 2344-2353. doi:10.1096/fj.10-174482

Che, M. X., Jiang, L. L., Li, H. Y., Jiang, Y. J. and Hu, H. Y. (2015). TDP-35 sequesters TDP-43 into cytoplasmic inclusions through binding with RNA. *FEBS Lett.* **589**, 1920-1928. doi:10.1016/j.febslet.2015.06.009

Chen, Y. and Cohen, T. J. (2019). Aggregation of the nucleic acid-binding protein TDP-43 occurs via distinct routes that are coordinated with stress granule formation. *J. Biol. Chem.* **294**, 3696-3706. doi:10.1074/jbc.RA118.006351

Chhangani, D., Martin-Pena, A. and Rincon-Limas, D. E. (2021). Molecular, functional, and pathological aspects of TDP-43 fragmentation. *iScience* **24**, 102459. doi:10.1016/j.isci.2021.102459

Chiti, F. and Dobson, C. M. (2017). Protein misfolding, amyloid formation, and human disease: a summary of progress over the last decade. *Annu. Rev. Biochem.* **86**, 27-68. doi:10.1146/annurev-biochem-061516-045115

Clarke, J. P., Thibault, P. A., Salapa, H. E. and Levin, M. C. (2021). A comprehensive analysis of the role of hnRNP A1 function and dysfunction in the pathogenesis of neurodegenerative disease. *Front. Mol. Biosci.* **8**, 659610. doi:10.3389/fmolb.2021.659610

Clery, A., Blatter, M. and Allain, F. H. (2008). RNA recognition motifs: boring? Not quite. *Curr. Opin. Struct. Biol.* **18**, 290-298. doi:10.1016/j.sbi.2008.04.002

Droppelmann, C. A., Campos-Melo, D., Moszczynski, A. J., Amzil, H. and Strong, M. J. (2019). TDP-43 aggregation inside micronuclei reveals a potential mechanism for protein inclusion formation in ALS. *Sci. Rep.* **9**, 19928. doi:10.1038/s41598-019-56483-y

Dugger, B. N. and Dickson, D. W. (2017). Pathology of neurodegenerative diseases. *Cold Spring Harb. Perspect Biol.* **9**, a028035. doi:10.1101/cshperspect.a028035

Elden, A. C., Kim, H. J., Hart, M. P., Chen-Plotkin, A. S., Johnson, B. S., Fang, X., Armakola, M., Geser, F., Greene, R., Lu, M. M. et al. (2010). Ataxin-2 intermediate-length polyglutamine expansions are associated with increased risk for ALS. *Nature* **466**, 1069-1075. doi:10.1038/nature09320

Franzmann, T. M. and Alberti, S. (2019). Prion-like low-complexity sequences: Key regulators of protein solubility and phase behavior. *J. Biol. Chem.* **294**, 7128-7136. doi:10.1074/jbc.TM118.001190

Freibaum, B. D., Chitta, R. K., High, A. A. and Taylor, J. P. (2010). Global analysis of TDP-43 interacting proteins reveals strong association with RNA splicing and translation machinery. *J. Proteome Res.* **9**, 1104-1120. doi:10.1021/pr901076y

Gregory, J. M., Barros, T. P., Meehan, S., Dobson, C. M. and Luheshi, L. M. (2012). The aggregation and neurotoxicity of TDP-43 and its ALS-associated 25 kDa fragment are differentially affected by molecular chaperones in Drosophila. *PLoS ONE* **7**, e31899. doi:10.1371/journal.pone.0031899

Harrison, A. F. and Shorter, J. (2017). RNA-binding proteins with prion-like domains in health and disease. *Biochem. J.* **474**, 1417-1438. doi:10.1042/BCJ20160499

Hartl, F. U. (2017). Protein Misfolding Diseases. *Annu. Rev. Biochem.* **86**, 21-26. doi:10.1146/annurev-biochem-061516-044518

Helder, S., Blythe, A. J., Bond, C. S. and Mackay, J. P. (2016). Determinants of affinity and specificity in RNA-binding proteins. *Curr. Opin. Struct. Biol.* **38**, 83-91. doi:10.1016/j.sbi.2016.05.005

Highet, B., Parker, R., Faull, R. L. M., Curtis, M. A. and Ryan, B. (2021). RNA Quality in post-mortem human brain tissue is affected by Alzheimer's disease. *Front. Mol. Neurosci.* **14**, 780352. doi:10.3389/fnmol.2021.780352

Hofmann, J. W., Seeley, W. W. and Huang, E. J. (2019). RNA Binding proteins and the pathogenesis of frontotemporal lobar degeneration. *Annu. Rev. Pathol.* **14**, 469-495. doi:10.1146/annurev-pathmechdis-012418-012955

Huang, Y. C., Lin, K. F., He, R. Y., Tu, P. H., Koubek, J., Hsu, Y. C. and Huang, J. J. (2013). Inhibition of TDP-43 aggregation by nucleic acid binding. *PLoS ONE* **8**, e64002. doi:10.1371/journal.pone.0064002

Ihara, R., Matsukawa, K., Nagata, Y., Kunugi, H., Tsuji, S., Chihara, T., Kuranaga, E., Miura, M., Wakabayashi, T., Hashimoto, T. et al. (2013). RNA binding mediates neurotoxicity in the transgenic Drosophila model of TDP-43 proteinopathy. *Hum. Mol. Genet.* **22**, 4474-4484. doi:10.1093/hmg/ddt296

Jiang, L. L., Che, M. X., Zhao, J., Zhou, C. J., Xie, M. Y., Li, H. Y., He, J. H. and Hu, H. Y. (2013). Structural transformation of the amyloidogenic core region of TDP-43 protein initiates its aggregation and cytoplasmic inclusion. *J. Biol. Chem.* **288**, 19614-19624. doi:10.1074/jbc.M113.463828

Jiang, L. L., Xue, W., Hong, J. Y., Zhang, J. T., Li, M. J., Yu, S. N., He, J. H. and Hu, H. Y. (2017). The N-terminal dimerization is required for TDP-43 splicing activity. *Sci. Rep.* **7**, 6196. doi:10.1038/s41598-017-06263-3

Johnson, J. O., Pioro, E. P., Boehringer, A., Chia, R., Feit, H., Renton, A. E., Pliner, H. A., Abramzon, Y., Marangi, G., Winborn, B. J. et al. (2014). Mutations in the Matrin 3 gene cause familial amyotrophic lateral sclerosis. *Nat. Neurosci.* **17**, 664-666. doi:10.1038/nn.3688

Kedersha, N. L., Gupta, M., Li, W., Miller, I. and Anderson, P. (1999). RNA-binding proteins TIA-1 and TIAR link the phosphorylation of eIF-2 alpha to the assembly of mammalian stress granules. *J. Cell Biol.* **147**, 1431-1442. doi:10.1083/jcb.147.7.1431

Kim, H. J., Kim, N. C., Wang, Y. D., Scarborough, E. A., Moore, J., Diaz, Z., MacLea, K. S., Freibaum, B., Li, S., Molliex, A. et al. (2013). Mutations in prion-like domains in hnRNPA2B1 and hnRNPA1 cause multisystem proteinopathy and ALS. *Nature* **495**, 467-473. doi:10.1038/nature11922

Kim, W., Kim, D. Y. and Lee, K. H. (2021). RNA-binding proteins and the complex pathophysiology of ALS. *Int. J. Mol. Sci.* **22**, 2598. doi:10.3390/ijms22052598

Lagier-Tourenne, C. and Cleveland, D. W. (2009). Rethinking ALS: the FUS about TDP-43. *Cell* **136**, 1001-1004. doi:10.1016/j.cell.2009.03.006

Lee, Y. B., Scotter, E. L., Lee, D. Y., Troakes, C., Mitchell, J., Rogelj, B., Gallo, J. M. and Shaw, C. E. (2021). Cytoplasmic TDP-43 is involved in cell fate during stress recovery. *Hum. Mol. Genet.* **31**, 166-175. doi:10.1093/hmg/ddab227

Liu, Y. and Shi, S. L. (2021). The roles of hnRNP A2/B1 in RNA biology and disease. *Wiley Interdiscip. Rev. RNA* **12**, e1612. doi:10.1002/wrna.1612

Lukavsky, P. J., Daujotyte, D., Tollervey, J. R., Ule, J., Stuani, C., Buratti, E., Baralle, F. E., Damberger, F. F. and Allain, F. H. (2013). Molecular basis of UG-rich RNA recognition by the human splicing factor TDP-43. *Nat. Struct. Mol. Biol.* **20**, 1443-1449. doi:10.1038/nsmb.2698

Mackenzie, I. R., Nicholson, A. M., Sarkar, M., Messing, J., Purice, M. D., Pottier, C., Annu, K., Baker, M., Perkerson, R. B., Kurti, A. et al. (2017). TIA1 Mutations in amyotrophic lateral sclerosis and frontotemporal dementia promote phase separation and alter stress granule dynamics. *Neuron* **95**, 808-816. doi:10.1016/j.neuron.2017.07.025

Mann, J. R., Gleixner, A. M., Mauna, J. C., Gomes, E., DeChellis-Marks, M. R., Needham, P. G., Copley, K. E., Hurtle, B., Portz, B., Pyles, N. J. et al. (2019). RNA Binding antagonizes neurotoxic phase transitions of TDP-43. *Neuron* **102**, 321-338. doi:10.1016/j.neuron.2019.01.048

Medina, D. X., Orr, M. E. and Oddo, S. (2014). Accumulation of C-terminal fragments of transactive response DNA-binding protein 43 leads to synaptic loss and cognitive deficits in human TDP-43 transgenic mice. *Neurobiol. Aging* **35**, 79-87. doi:10.1016/j.neurobiolaging.2013.07.006

Mehta, A. R., Selvaraj, B. T., Barton, S. K., McDade, K., Abrahams, S., Chandran, S., Smith, C. and Gregory, J. M. (2020). Improved detection of RNA

foci in C9orf72 amyotrophic lateral sclerosis post-mortem tissue using BaseScope shows a lack of association with cognitive dysfunction. *Brain Commun.* **2**, fcaa009. doi:10.1093/braincomms/fcaa009

Meyer, C., Garzia, A., Mazzola, M., Gerstberger, S., Molina, H. and Tuschl, T. (2018). The TIA1 RNA-binding protein family regulates EIF2AK2-mediated stress response and cell cycle progression. *Mol. Cell* **69**, 622-635. doi:10.1016/j.molcel.2018.01.011

Mompean, M., Romano, V., Pantoja-Uceda, D., Stuani, C., Baralle, F. E., Buratti, E. and Laurents, D. V. (2017). Point mutations in the N-terminal domain of transactive response DNA-binding protein 43 kDa (TDP-43) compromise its stability, dimerization, and functions. *J. Biol. Chem.* **292**, 11992-12006. doi:10.1074/jbc.M117.775965

Neumann, M., Sampathu, D. M., Kwong, L. K., Truax, A. C., Micsenyi, M. C., Chou, T. T., Bruce, J., Schuck, T., Grossman, M., Clark, C. M. et al. (2006). Ubiquitinated TDP-43 in frontotemporal lobar degeneration and amyotrophic lateral sclerosis. *Science* **314**, 130-133. doi:10.1126/science.1134108

Nishimoto, Y., Ito, D., Yagi, T., Nihei, Y., Tsunoda, Y. and Suzuki, N. (2010). Characterization of alternative isoforms and inclusion body of the TAR DNA-binding protein-43. *J. Biol. Chem.* **285**, 608-619. doi:10.1074/jbc.M109.022012

Nussbacher, J. K., Tabet, R., Yeo, G. W. and Lagier-Tourenne, C. (2019). Disruption of RNA Metabolism in Neurological Diseases and Emerging Therapeutic Interventions. *Neuron* **102**, 294-320. doi:10.1016/j.neuron.2019.03.014

Passoni, M., De Conti, L., Baralle, M. and Buratti, E. (2012). UG repeats/TDP-43 interactions near 5′ splice sites exert unpredictable effects on splicing modulation. *J. Mol. Biol.* **415**, 46-60. doi:10.1016/j.jmb.2011.11.003

Patel, R. C. and Sen, G. C. (1998). PACT, a protein activator of the interferon-induced protein kinase, PKR. *EMBO J.* **17**, 4379-4390. doi:10.1093/emboj/17.15.4379

Pesiridis, G. S., Tripathy, K., Tanik, S., Trojanowski, J. Q. and Lee, V. M. (2011). A "two-hit" hypothesis for inclusion formation by carboxyl-terminal fragments of TDP-43 protein linked to RNA depletion and impaired microtubule-dependent transport. *J. Biol. Chem.* **286**, 18845-18855. doi:10.1074/jbc.M111.231118

Picchiarelli, G. and Dupuis, L. (2020). Role of RNA binding proteins with prion-like domains in muscle and neuromuscular diseases. *Cell Stress* **4**, 76-91. doi:10.15698/cst2020.04.217

Rhine, K., Vidaurre, V. and Myong, S. (2020). RNA Droplets. *Annu. Rev. Biophys.* **49**, 247-265. doi:10.1146/annurev-biophys-052118-115508

Sanchez-Jimenez, C. and Izquierdo, J. M. (2015). T-cell intracellular antigens in health and disease. *Cell Cycle* **14**, 2033-2043. doi:10.1080/15384101.2015.1053668

Smethurst, P., Sidle, K. C. and Hardy, J. (2015). Review: Prion-like mechanisms of transactive response DNA binding protein of 43 kDa (TDP-43) in amyotrophic lateral sclerosis (ALS). *Neuropathol. Appl. Neurobiol.* **41**, 578-597. doi:10.1111/nan.12206

Suk, T. R. and Rousseaux, M. W. C. (2020). The role of TDP-43 mislocalization in amyotrophic lateral sclerosis. *Mol. Neurodegener.* **15**, 45. doi:10.1186/s13024-020-00397-1

Tank, E. M., Figueroa-Romero, C., Hinder, L. M., Bedi, K., Archbold, H. C., Li, X., Weskamp, K., Safren, N., Paez-Colasante, X., Pacut, C. et al. (2018). Abnormal RNA stability in amyotrophic lateral sclerosis. *Nat. Commun.* **9**, 2845. doi:10.1038/s41467-018-05049-z

Tollervey, J. R., Curk, T., Rogelj, B., Briese, M., Cereda, M., Kayikci, M., Konig, J., Hortobagyi, T., Nishimura, A. L., Zupunski, V. et al. (2011). Characterizing the RNA targets and position-dependent splicing regulation by TDP-43. *Nat. Neurosci.* **14**, 452-458. doi:10.1038/nn.2778

Toyoshima, Y., Tanaka, H., Shimohata, M., Kimura, K., Morita, T., Kakita, A. and Takahashi, H. (2011). Spinocerebellar ataxia type 2 (SCA2) is associated with TDP-43 pathology. *Acta Neuropathol.* **122**, 375-378. doi:10.1007/s00401-011-0862-7

Vivoli-Vega, M., Guri, P., Chiti, F. and Bemporad, F. (2020). Insight into the folding and dimerization mechanisms of the N-Terminal domain from human TDP-43. *Int. J. Mol. Sci.* **21**, 6259. doi:10.3390/ijms21176259

Waris, S., Wilce, M. C. and Wilce, J. A. (2014). RNA recognition and stress granule formation by TIA proteins. *Int. J. Mol. Sci.* **15**, 23377-23388. doi:10.3390/ijms151223377

Waris, S., Garcia-Maurino, S. M., Sivakumaran, A., Beckham, S. A., Loughlin, F. E., Gorospe, M., Diaz-Moreno, I., Wilce, M. C. J. and Wilce, J. A. (2017). TIA-1 RRM23 binding and recognition of target oligonucleotides. *Nucleic Acids Res.* **45**, 4944-4957. doi:10.1093/nar/gkx102

Winton, M. J., Igaz, L. M., Wong, M. M., Kwong, L. K., Trojanowski, J. Q. and Lee, V. M. (2008). Disturbance of nuclear and cytoplasmic TAR DNA-binding protein (TDP-43) induces disease-like redistribution, sequestration, and aggregate formation. *J. Biol. Chem.* **283**, 13302-13309. doi:10.1074/jbc.M800342200

Wolozin, B. and Ivanov, P. (2019). Stress granules and neurodegeneration. *Nat. Rev. Neurosci.* **20**, 649-666. doi:10.1038/s41583-019-0222-5

Wood, A., Gurfinkel, Y., Polain, N., Lamont, W. and Lyn Rea, S. (2021). Molecular mechanisms underlying TDP-43 pathology in cellular and animal models of ALS and FTLD. *Int. J. Mol. Sci.* **22**, 4705. doi:10.3390/ijms22094705

Xiao, S., Sanelli, T., Chiang, H., Sun, Y., Chakrabartty, A., Keith, J., Rogaeva, E., Zinman, L. and Robertson, J. (2015). Low molecular weight species of TDP-43 generated by abnormal splicing form inclusions in amyotrophic lateral sclerosis and result in motor neuron death. *Acta Neuropathol.* **130**, 49-61. doi:10.1007/s00401-015-1412-5

Xue, W., Zhang, S.-X., He, W.-T., Hong, J.-Y., Jiang, L.-L. and Hu, H.-Y. (2020a). Domain interactions reveal auto-inhibition of the deubiquitinating enzyme USP19 and its activation by HSP90 in the modulation of huntingtin aggregation. *Biochem. J.* **477**, 4295-4312. doi:10.1042/BCJ20200536

Xue, Y. C., Ng, C. S., Xiang, P., Liu, H., Zhang, K., Mohamud, Y. and Luo, H. (2020b). Dysregulation of RNA-binding proteins in amyotrophic lateral sclerosis. *Front Mol Neurosci* **13**, 78. doi:10.3389/fnmol.2020.00078

Yang, H. and Hu, H. Y. (2016). Sequestration of cellular interacting partners by protein aggregates: implication in a loss-of-function pathology. *FEBS J.* **283**, 3705-3717. doi:10.1111/febs.13722

Yang, H., Li, J.-J., Liu, S., Zhao, J., Jiang, Y.-J., Song, A.-X. and Hu, H.-Y. (2014). Aggregation of polyglutamine-expanded ataxin-3 sequesters its specific interacting partners into inclusions: implication in a loss-of-function pathology. *Sci. Rep.* **4**, 6410. doi:10.1038/srep06410

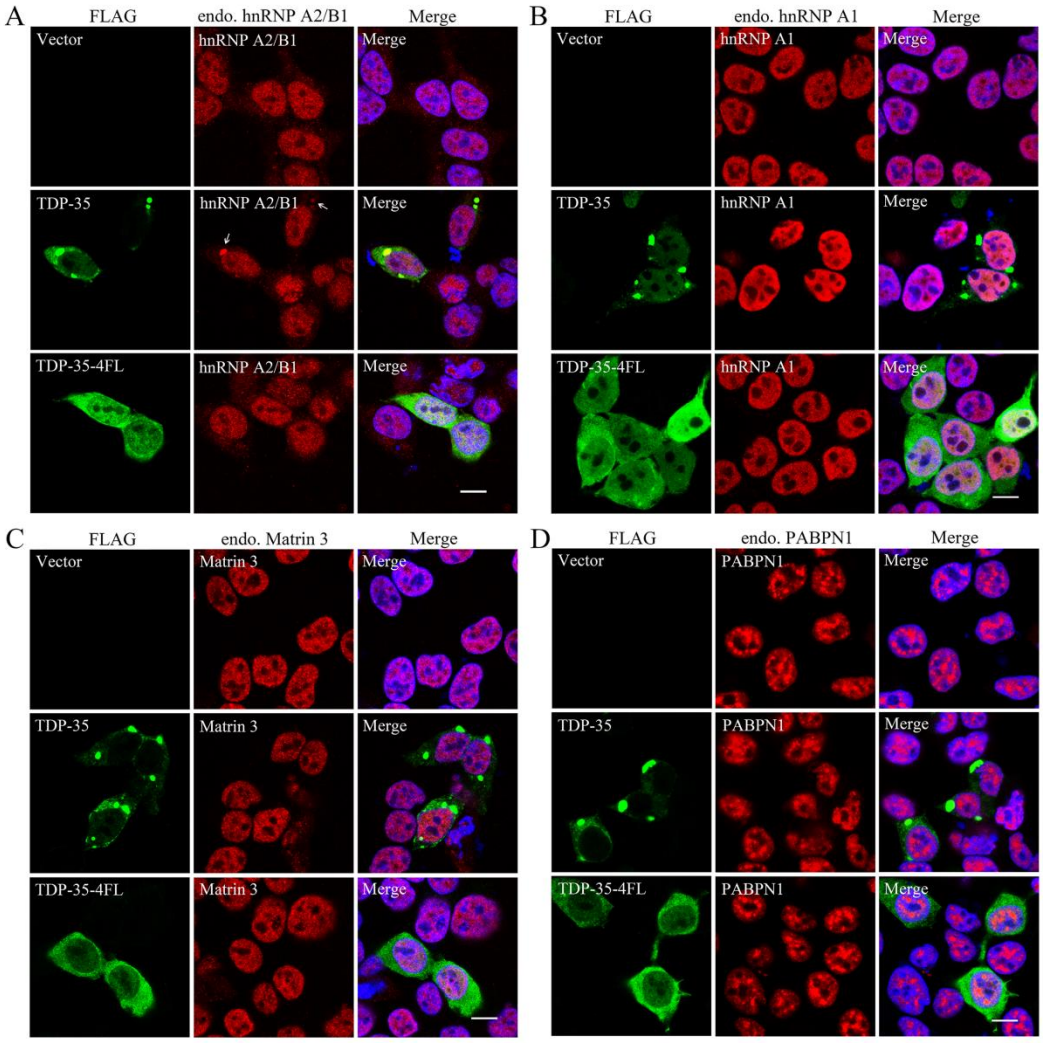

Fig. S1. Characterization of the RBPs sequestered by the cytoplasmic TDP-35 inclusions by immunofluorescence imaging

(**A**) Identification of hnRNP A2B1 that co-localizes with the inclusions. (**B**, **C**, **D**) hnRNP A1 (B), Matr3 (C) or PABPN1 (D) that does not co-localize with the inclusions. The HEK 293T cells expressing FLAG vector, FLAG-TDP-35 or FLAG-TDP-35-4FL were imaged, and the endogenous RBPs were examined with the indicated antibodies. TDP-35 and its mutant were stained with anti-FLAG antibody (green), RBPs were stained with indicated antibodies (red), and the nuclei were stained with Hoechst (blue). Scale bar = 10 μm.

Journal of Cell Science • Supplementary information

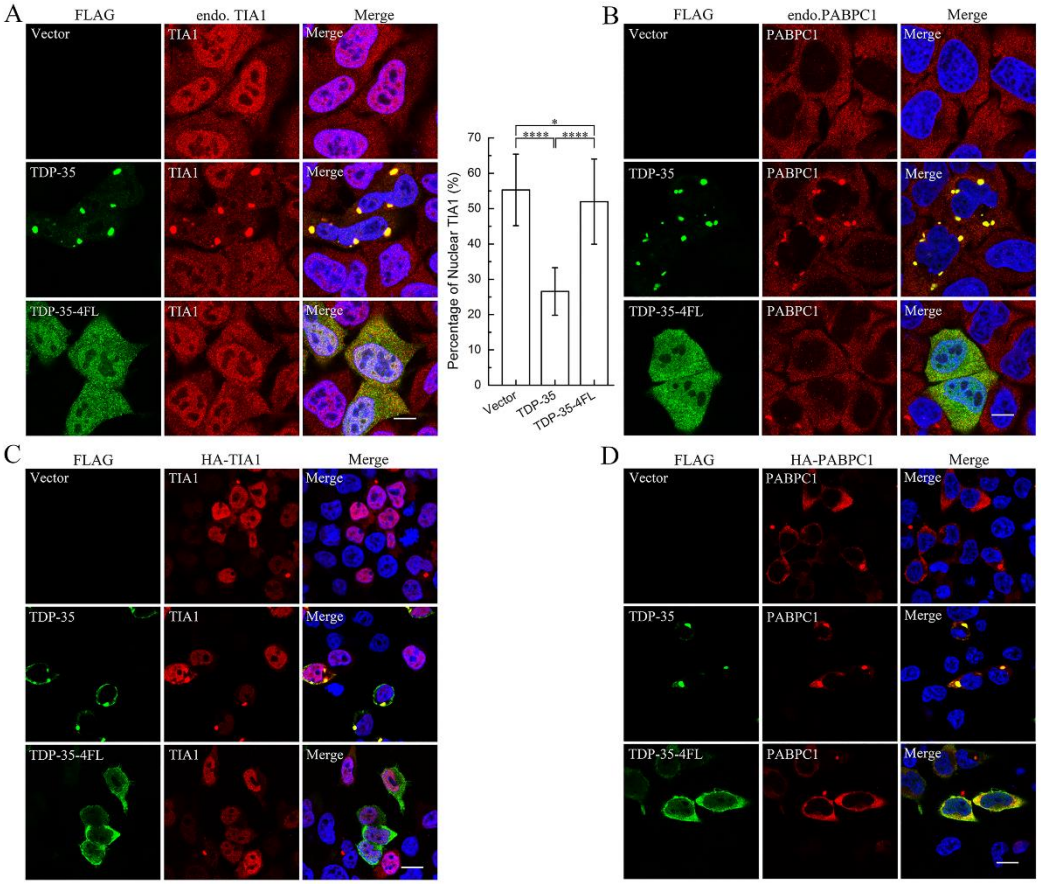

Fig. S2. Confirmation of TIA1 and PABPC1 co-localized with the cytoplasmic TDP-35 inclusions by immunofluorescence imaging

(**A**, **B**) Co-localization of endogenous TIA1 and PABPC1 with the cytoplasmic TDP-35 inclusions in HeLa cells. The HeLa cells over-expressing FLAG vector, FLAG-TDP-35 or FLAG-TDP-35-4FL were imaged, and the endogenous TIA1 (A) or PABPC1 (B) was shown to be co-localized with the cytoplasmic TDP-35 inclusions. FLAG-TDP-35-4FL was set as a control. The inset graph shown in (A) is the percentage of nuclear TIA1 in the cells with TDP-35 inclusions. The amounts of nuclear and total TIA1 were obtained from the pixel intensities of individual cell image, and the data were statistically analyzed by one-way ANOVA and presented as Means ± SEM (Vector, n=36; TDP-35, n=35; TDP-35-4FL, n=24). *, $p < 0.05$, ****, $p < 0.0001$. **(C**, **D)** Co-localization of exogenous TIA1 or PABPC1 with the cytoplasmic TDP-35 inclusions in HEK 293T cells. HA-TIA1 (C) or HA-PABPC1 (D) was co-transfected with FLAG-TDP-35 in HEK 293T cells, and the cells were visualized by immunofluorescence imaging. TDP-35 and its mutant were stained with anti-FLAG antibody (green). Endogenous TIA1 or PABPC1 was stained with antibody anti-TIA1 or anti-PABP antibody (red), while exogenous HA-tagged TIA1 or PABPC1 was stained with anti-HA antibody (red). The nuclei were stained with Hoechst (blue). Scale bar = 10 μm.

Journal of Cell Science • Supplementary information

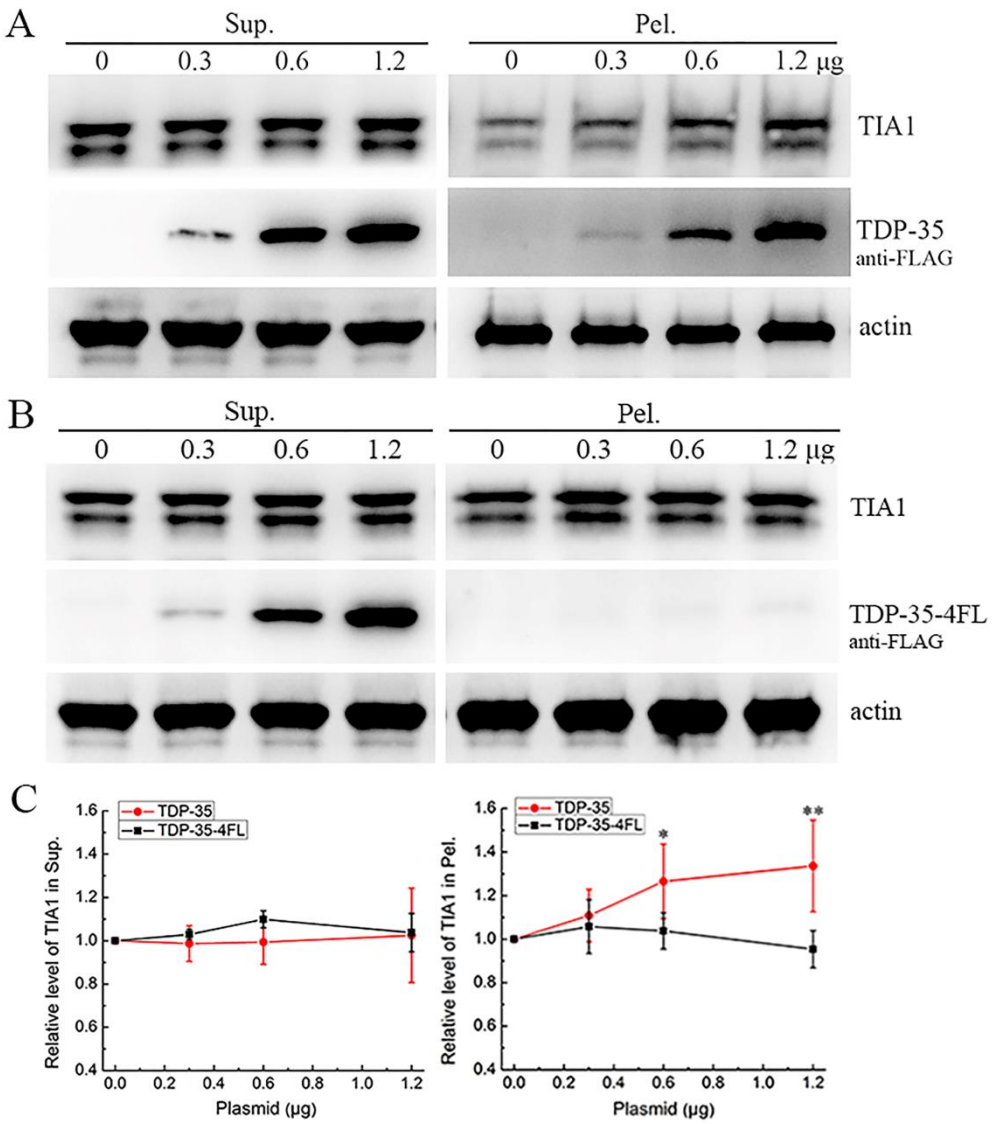

Fig. S3. Dose-dependent experiment for characterizing the sequestration of endogenous TIA1 by the TDP-35 aggregates

(**A**) Sequestration of endogenous TIA1 by TDP-35. (**B**) By TDP-35-4FL as a control. HeLa cells were transfected with different dose of the FLAG-TDP-35 (A) or FLAG-TDP-35-4FL (B) plasmid, and the cell lysates were subjected to supernatant/pellet fractionation and Western blotting analysis for TIA1. The proteins were detected by using anti-FLAG, anti-TIA1 and anti-actin antibodies. (**C**) Quantification of the amounts of TIA1 in supernatant and pellet fractions. Data are shown as Means ±SEM (n=3). *, $p<0.05$; **, $p<0.01$. Sup., supernatant; Pel., pellet.

Journal of Cell Science • Supplementary information

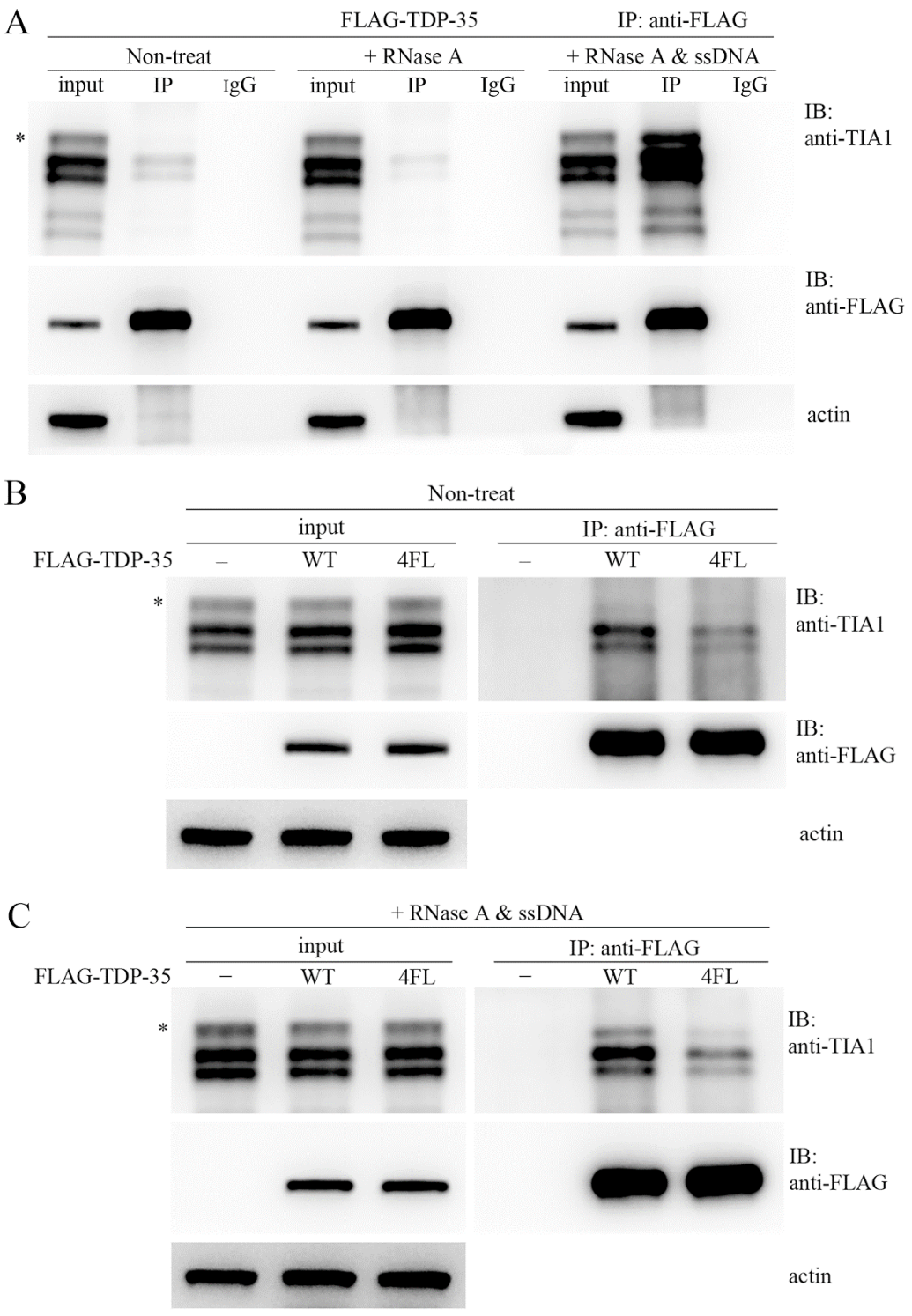

Journal of Cell Science • Supplementary information

Fig. S4. TDP-35 associates with endogenous TIA1 mediated by sequence-specific RNA.

(**A**) Immunoprecipitation experiment examining the effects of RNase and ssDNA treatments on the association of FLAG-TDP-35 with endogenous TIA1. The cell lysates were immunoprecipitated with protein A/G beads plus FLAG antibody under various conditions including non-treat, RNase treatment, and RNase A plus ssDNA treatment. IgG, a control without FLAG antibody; IP, with anti-FLAG antibody. The immunoblotting was carried out with an antibody against either TIA1 or FLAG. ssDNA, TG+TC. *, non-specific band. (**B**) Immunoprecipitation for association of FLAG-TDP-35 or FLAG-TDP-35-4FL with endogenous TIA1. The lysates were immunoprecipitated with protein A/G beads plus FLAG antibody under the condition of non-treat and then immunoblotted with an antibody against either TIA1 or FLAG. (**C**) Immunoprecipitation for ssDNA-assisted association of FLAG-TDP-35 with endogenous TIA1. FLAG-TDP-35-4FL was set as a control. The lysates were immunoprecipitated with protein A/G beads plus FLAG antibody and subjected to RNase and ssDNA (TG+TC) treatments, and then immunoblotted with the indicated antibodies. In all IP experiments, about 8% loading of the sample was applied for input.

Journal of Cell Science • Supplementary information

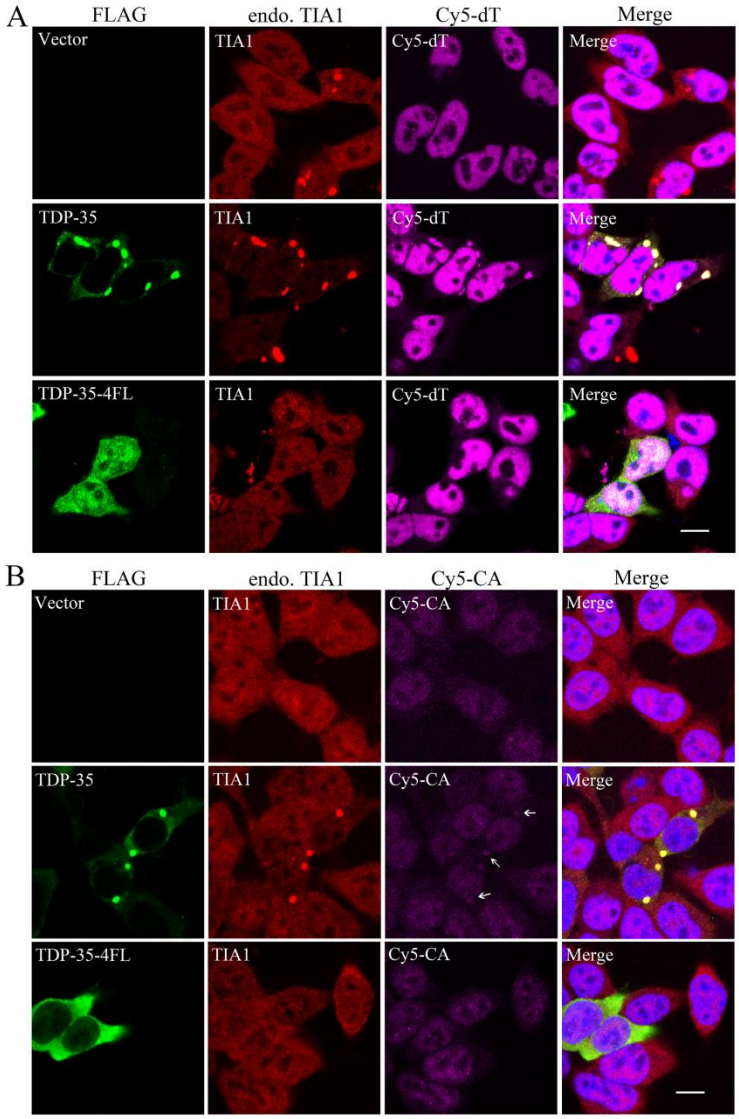

Fig. S5. Combined FISH and IF experiment for detecting specific RNAs enriched in the TDP-35 inclusions in HEK 293T cells.

(**A**) Imaging with the Cy5-oligo-dT probe showing poly(A)-containing RNAs enriched in the cytoplasmic TDP-35 inclusions co-localized with endogenous TIA1. (**B**) Imaging with the Cy5-CA probe showing UG-repeat RNAs in the inclusions co-localized with endogenous TIA1. FLAG-TDP-35 and FLAG-TDP-35-4FL are in green, TIA1 is in red, RNAs are in pink, while the nuclei are in blue (DAPI). Scale bar = 10 μm.

Journal of Cell Science • Supplementary information

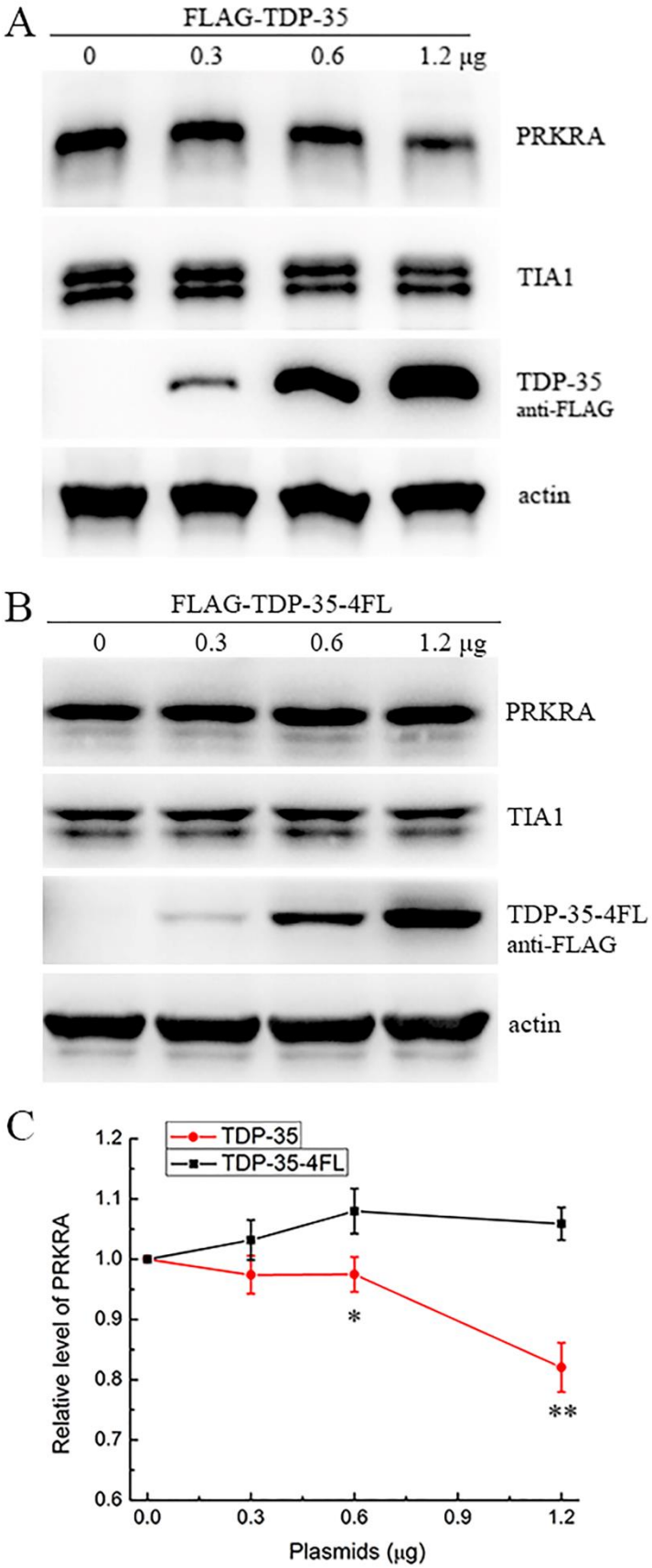

Journal of Cell Science • Supplementary information

Fig. S6. Dose-dependent experiment for characterizing the effect of TDP-35 on the protein level of PRKRA.

(**A**) Effect of TDP-35 over-expression on the PRKRA level. (**B**) TDP-35-4FL as a control. (**C**) Qualification of the alteration of the PRKRA level. HeLa cells were transfected with each indicated plasmid, the cell lysates were centrifuged, and then the supernatant was subjected to Western blotting analysis. Data are shown as Means ± SEM (n=3). *, $p<0.05$; **, $p<0.01$.

Journal of Cell Science • Supplementary information

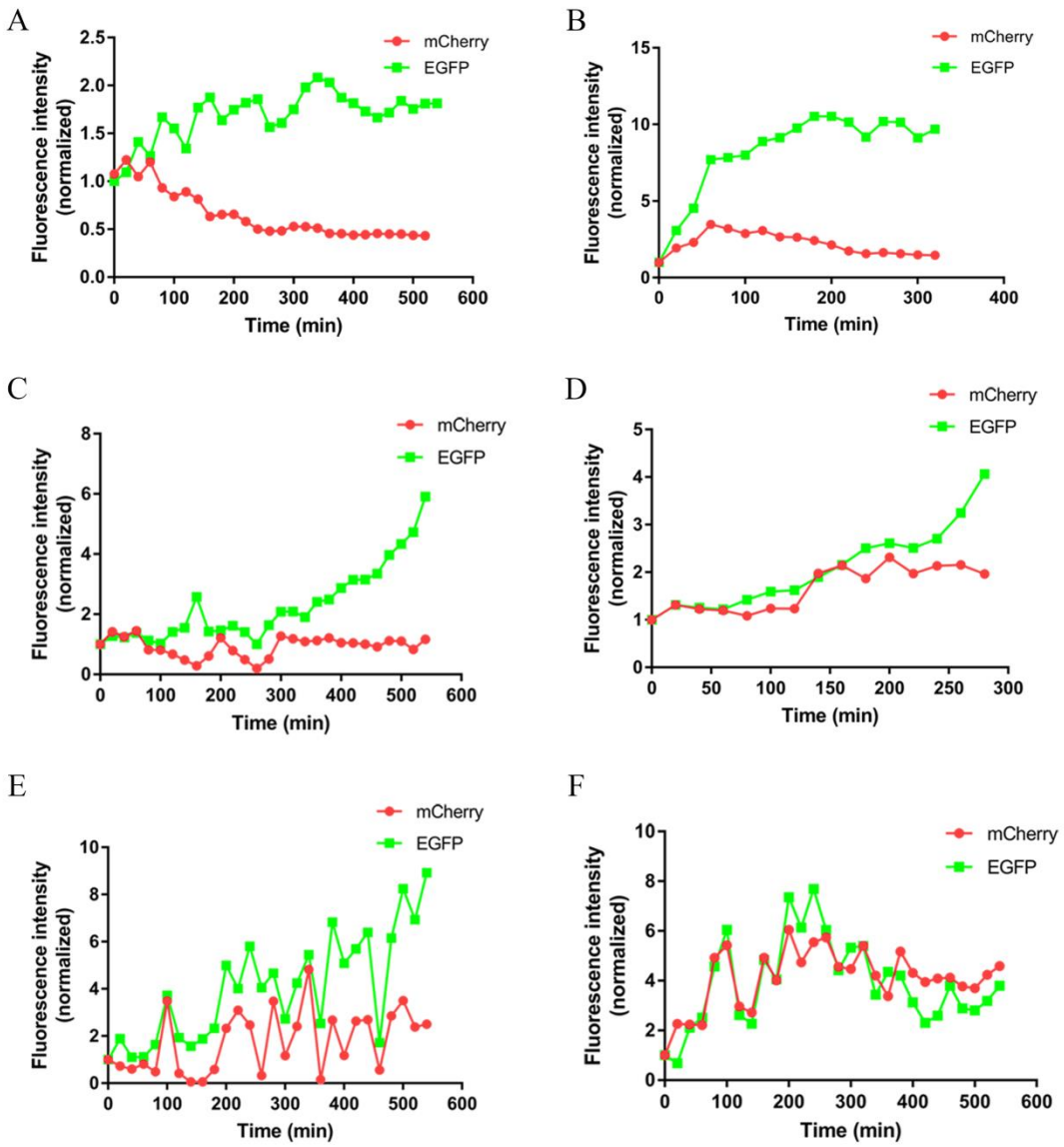

Fig. S7. Quantification of the fluorescence intensities of mCherry and EGFP for individual inclusions in a time-lapse movie.

Six graphs are extracted from the movie and each stand for an individual inclusion. The intensity data are normalized to that of the 0-min point.

Journal of Cell Science • Supplementary information

Table S1. List of the constructs applied in this study.

Constructs	Vectors	Restriction Enzyme sites	Additional
FLAG-TDP-35	FLAG-pcDNA3.1	BamH I / Xho I	TDP-35, residues 90-414 of TDP-43
mCherry-TDP-35	FLAG-pcDNA3.1	Hind III / BamH I	TDP-35, N-terminally tagged mCherry
TDP-35-mCherry	FLAG-pcDNA3.1	BamH I / Xho I	TDP-35, C-terminally tagged mCherry
FLAG-TDP-35-4FL	FLAG-pcDNA3.1	BamH I / Xho I	TDP-35, RRM mutant: F147/149/229/231L
HA-TIA1	HA-pcDNA3.0	BamH I / Xho I	Full-length TIA1, isoform 1
HA-PABPC1	HA-pcDNA3.0	BamH I / Xho I	Full-length PABPC1
Cas9-sgRNA(TDP-43)-mCherry EGFP-TDP-43	pX330 FLAG-pcDNA3.1	Bpi I BamH I / Xho I	For constructing an EGFP-TDP-43 cell line by CRISPR/Cas9

Journal of Cell Science • Supplementary information

Table S2. List of the antibodies used in this study.

Antibody	Source	Catalog Number	Dilution
Anti-FLAG (mouse)	Sigma-Aldrich	F1804	WB: 1:1000 IF: 1:200 IP: 1:1000
Anti-FLAG (rabbit)	Proteintech	20543-1-AP	WB: 1:1000 IF: 1:200
Anti-HA (mouse)	Sigma-Aldrich	H9658	WB: 1:1000 IF: 1:200
Anti-TIA1 (mouse)	Santa Cruz Biotechnology	sc-166247	WB: 1:1000 IF: 1:100
Anti-TIA1 (rabbit)	Proteintech	12133-2-AP	WB: 1:3000 IF: 1:200
Anti-PABP (rabbit, for PABPC1)	Abcam	ab21060	IF: 1:100
Anti-Matrin 3 (rabbit)	Abcam	ab151714	IF: 1:200
Anti-PABPN1 (rabbit)	Abcam	ab75855	IF: 1:200
Anti- hnRNP A2/B1 (rabbit)	Proteintech	14813-1-AP	IF: 1:200
Anti-hnRNP A1 (mouse)	Santa Cruz Biotechnology	sc-32301	IF: 1:100
Anti-PACT (mouse, for PRKRA)	Santa Cruz Biotechnology	sc-377103	WB: 1:1000
Anti-β-actin (mouse)	Proteintech	6008-1-Ig	WB: 1:5000

WB, Western blotting; IF, immunofluorescence. IP, immunoprecipitation.

Journal of Cell Science • Supplementary information

Table S3. Nucleotide sequences of ssDNAs, FISH probes and RT-PCR primers applied in this study.

ssDNA/probe /primer	Sequence
TG (58 nt)	5'-TGTGTGTGTGTGTGTGTGTGTGTGTGTGTGTGTGTGTGTGTGTGTGTG-3'
TC (30 nt)	5'-TTTTTACTCCCCTCATTTTTTTTTTACTCC-3'
TG+TC (78 nt)	5'-TGTGTGTGTGTGTGTGTGTGTGTGTGTGTGTGTGTGTGTGTGTGTGTTTTACTCCCCTCATTTTTTTTTTACTCC-3'
Cy5-oligo dT	Cy5-5'-TTTTTTTTTTTTTTTTTTTTTTTTT-3'
Cy5-CA	Cy5-5'- CACACACACACACACACACACACA -3'
Cy5-NN	Cy5-5'- NNNNNNNNNNNNNNNNNNNNNNNN-3'
GAPDH-forward GAPDH-reverse	5'-GGAGCGAGATCCCTCCAAAAT-3' 5'-GGCTGTTGTCATACTTCTCATGG-3'
PRKRA-forward PRKRA-reverse	5'-GTGAAGGTACAAGTAAGAAGCTGGCG-3' 5'-AATGAACCAATAGGATTAAGCTGGTTCTTT-3'

Journal of Cell Science • Supplementary information

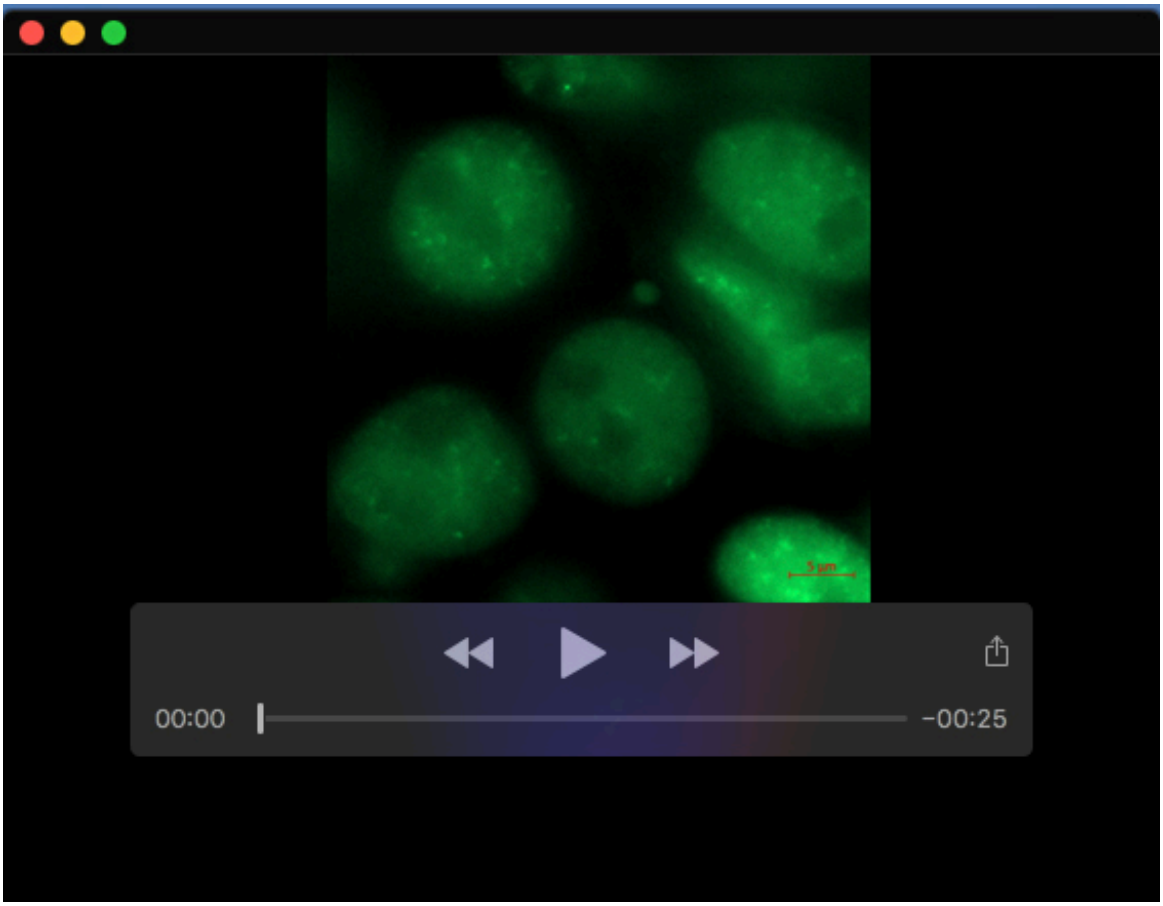

Movie 1. Time-lapse movie for sequestration of TDP-43 over-expressing FLAG-TDP-35. Movie related to Fig. 6B.

The movie was imaged with 20-min intervals in the EGFP-TDP-43 cell line transfected with FLAG-TDP-35. The imaging began at c.a. 12 hrs after transfection with FLAG-TDP-35. TDP-43 was indicated from the fluorescence of its fused EGFP (green). The live-cell images were obtained by Zeiss Celldiscoverer 7 (Zeiss). Scale bar, 5 μm.

Journal of Cell Science • Supplementary information

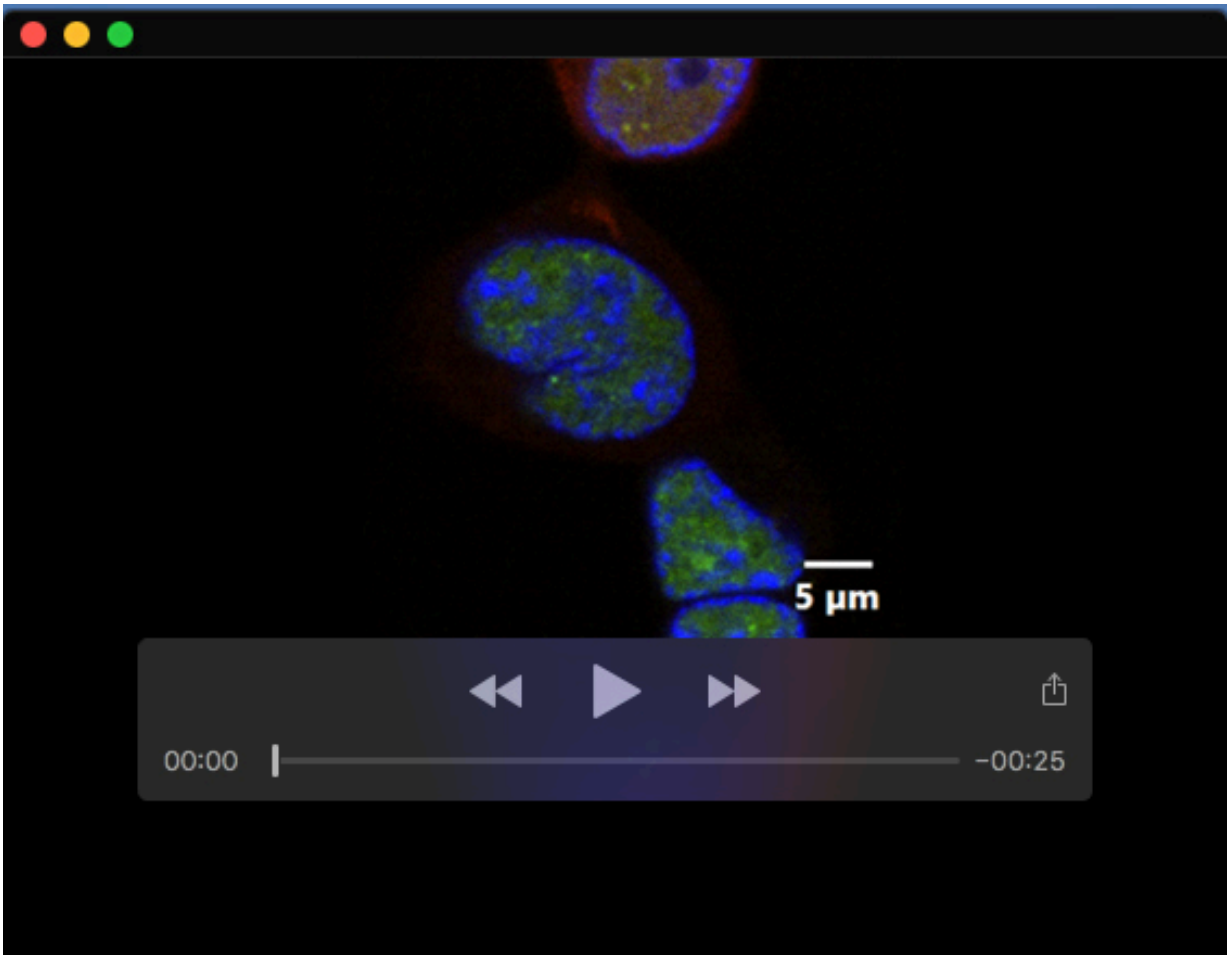

Movie 2. Time-lapse movie for sequestration of TDP-43 over-expressing TDP-35-mCherry. Movie related to Fig. 7A.

The movie was imaged with 20-min intervals in the EGFP-TDP-43 cell line transfected with TDP-35-mCherry. The imaging began at c.a. 12 hrs after transfection with TDP-35-mCherry. TDP-43 was indicated from the fluorescence of its fused EGFP (green), while TDP-35 was lighted up by the fluorescence of its fused mCherry (red), and nuclei were stained with Hoechst (blue). The live-cell images were obtained by Olympus SpinSR (Olympus), Scale bar = 5 µm.

Journal of Cell Science • Supplementary information